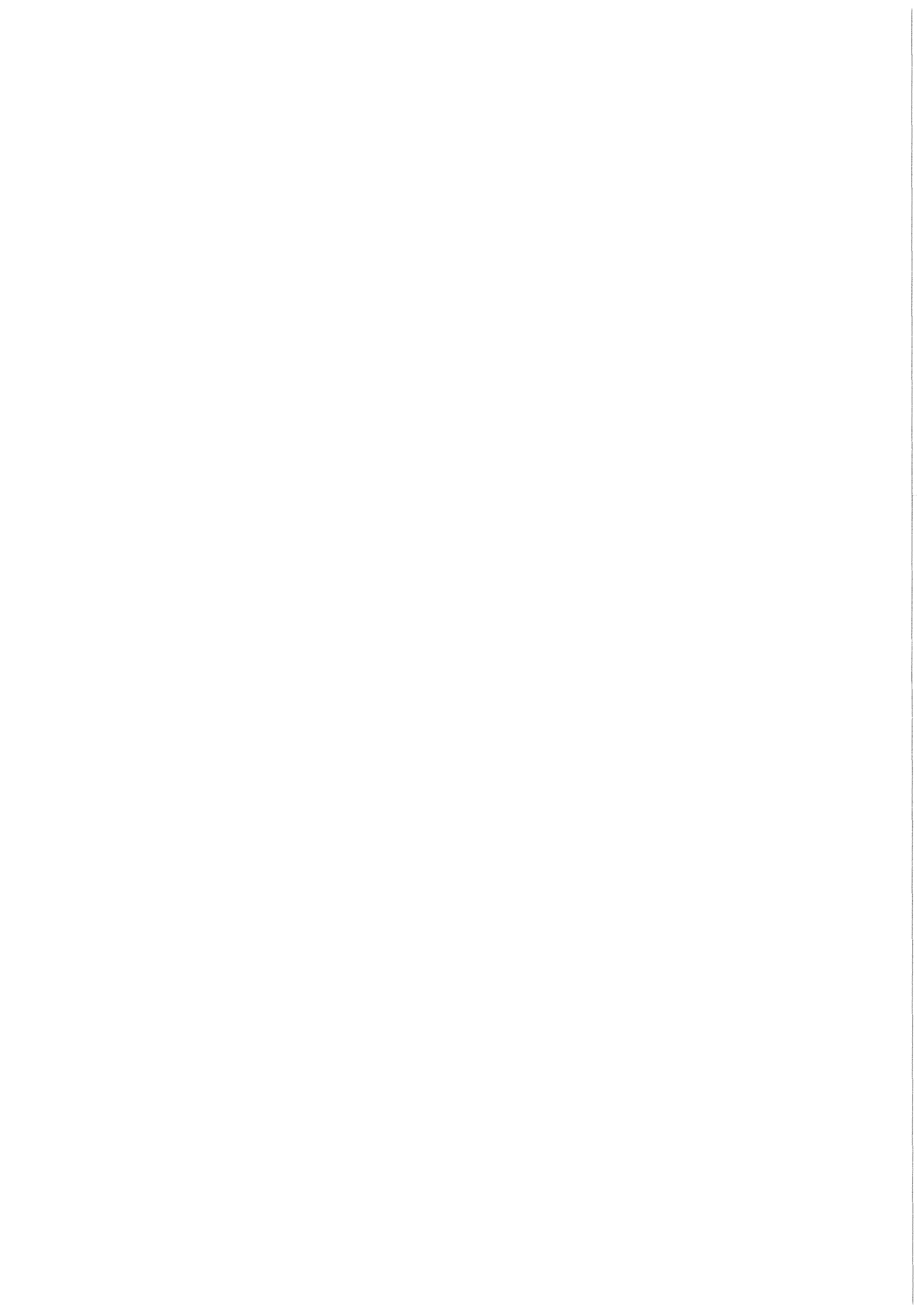


KfK 3592
Oktober 1983

Freezing of Aluminium Oxide and Iron Flowing Upward in Circular Quartz Glass Tubes

D. Kuhn, M. Mösche, H. Werle
Institut für Neutronenphysik und Reaktortechnik
Projekt Schneller Brüter

Kernforschungszentrum Karlsruhe



KERNFORSCHUNGSZENTRUM KARLSRUHE
Institut für Neutronenphysik und Reaktortechnik
Projekt Schneller Brüter

KfK 3592

Freezing of Aluminium Oxide and Iron
Flowing Upward in Circular Quartz
Glass Tubes

D. Kuhn, M. Möschke, H. Werle

Kernforschungszentrum Karlsruhe GmbH, Karlsruhe

Als Manuskript vervielfältigt
Für diesen Bericht behalten wir uns alle Rechte vor

Kernforschungszentrum Karlsruhe GmbH
ISSN 0303-4003

Summary

The freezing of aluminium oxide and iron flowing upward in circular quartz glass tubes has been studied in a series of experiments. Several tubes were used in the same test. This demonstrated a good reproducibility and allowed systematic parameter variations, especially of the channel diameter. The time-dependance of the penetration was observed with a film camera and these data provide a good basis for a detailed check of sophisticated models which are in development.

Ausfrieren von in zylindrischen Quarzglas-Rohren nach oben strömendem Aluminiumoxid und Eisen

Zusammenfassung

Das Ausfrieren von in zylindrischen Quarzglas-Rohren nach oben strömendem Aluminiumoxid und Eisen wurde in einer Reihe von Experimenten untersucht. Pro Test wurden mehrere Rohre verwendet. Damit konnte eine gute Reproduzierbarkeit nachgewiesen und systematische Parameteruntersuchungen, insbesondere hinsichtlich des Kanaldurchmessers, durchgeführt werden. Der Zeitverlauf des Eindringens wurde mit einer Filmkamera registriert. Diese Aufnahmen liefern eine gute Basis für eine detaillierte Überprüfung der theoretischen Modelle, die derzeit entwickelt werden.

1. Introduction

An important problem in fast reactor safety analysis is to determine the behaviour of molten fuel as it moves into the axial blanket during a core disruptive accident. If a significant fraction of the core fuel inventory can move into or beyond the axial blankets, the probability of avoiding recriticality and achieving early accident termination is greatly increased.

Many studies have been performed in the last years addressing freezing processes that may occur under conditions applicable to the flow and freezing of molten core material. A thorough review has recently been made by Greene and Barry /1/. Most of the experimental studies were performed at low temperatures using simulant materials. Only a few were conducted at conditions representative for reactor accidents. In the uranium thermite tests of ANL /2/, the melt was a mixture of metal and UO_2 with a high void fraction and the test section was in most cases a complicated pin bundle simulating the axial blanket. In the COCOTTE experiments of Grenoble /3/, freezing dynamics of single-phase UO_2 in circular tubes and pin bundles was investigated. Both of these reactor representative studies were relative expensive and therefore tests of reproducibility and systematic parameter variations have not been made.

It was the goal of the present study to perform a series of experiments which are at least in some respects (melt material, high temperature) representative for reactor accident conditions and which are, on the other hand, suited for comparison with theoretical models. This requires firstly that the experimental data are reproducible. Secondly, a larger number of quantitative data and preferably such where some important parameters are varied systematically, are needed. In addition, both, the melt and the test section, should be sufficiently simple that the codes can handle it. For these reasons, single-phase (zero void fraction) aluminium oxide

or iron, generated by the thermite reaction, were used as melt. The test section consisted of one or more circular quartz glass tubes. This allows optical observation of the melt movement.

2. Experiments

2.1 Material properties

Commercial available welding thermite (type 10/R 70-SSH, manufactured May 19, 1982) was used in all but one experiment (No. 83/4/21-1). The thermite is ignited electrically with an igniter in ceramic crucibles (Al-Si-K-oxide, Tab. 1). The reaction lasts about 10 s and a few seconds later the two phases have separated (oxide above metal) and gases and vapor have been released.

The reaction products have been analysed by a scanning electron microscope (SEM). The metallic phase consists essentially of Fe, whereas the oxide phase is a mixture of Al-, Fe- and Si-oxide (Tab. 1). The Si stems mainly from

Properties of materials frozen in quartz glass tubes

	Metal	Oxide
Composition, At. %	Fe, 100	Al, 64 - 71 Fe, 20 - 27 Si, 7 - 10
Melting point (°C)	1510 ± 11	1830 ± 20

molten crucible material. The melting point of the metal has been determined with a carefully calibrated pyrometer and agrees with that for pure iron. The melting point of the oxide has been measured with a WRe thermocouple and the result is, according to the phase diagram of the system $\text{FeO-Al}_2\text{O}_3\text{-SiO}_2$, consistent with the composition.

2.2 Experimental setup

Quartz glass tubes (axis vertical, length 100 cm, wall thickness 1 mm) with different diameters are inserted from above into the crucible. The tubes are initially at room temperature and are surrounded by air with room temperature and atmospheric pressure. Shortly after dip in, a pressure difference Δp is applied between the inlet and the exit of the tubes, forcing the melt to flow into the tubes. Depending on the position of the tube inlet, either oxide or metal flows into the tube. If the inlet ends in the metal, but near the oxide/metal interface, the inflowing melt consists first of metal and then, because the interface sinks during flow, of oxide. Similar, if the inlet ends just below the liquid surface, the inflow may stop before plugging and the melt may deposit on the tube wall as a crust.

Three series of measurements have been performed. In the first series of measurements ("1 quartz glass tube") only one tube was inserted into the melt (350 g thermite), about 30 s after ignition. The crucible and the inlet of the tube were contained in a spherical vessel, the exit of the tube was at atmospheric pressure. The vessel was pressurized about 1 s after dip in.

The time dependance of the pressure difference was measured in a separate run (Fig. 1), but it is assumed, that is was similar in the freezing tests (Fig. 2 - 4). The temperature of the melt was not measured for this series, but it was estimated from the later series (Fig. 9 and 18) to be about 1800 ± 100 °C

during flow (32s after ignition). The results of this series should therefore not be used for quantitative comparisons.

The experimental setup for the next two series is shown in Fig. 5. The melt is forced to flow into the tubes by evacuating the tube exit. The time dependence of the pressure difference as well as the temperature of the melt is measured for each experiment. A W3Re/W25Re thermocouple sealed with quartz glass is used to measure the temperature of the melt. A computer controlled system is used to run the experiments and to collect the data. 23 s after ignition the tubes were inserted and 0.42 s later pressure was applied. In the second series 680 g thermite were used and 3 tubes were dipped into the melt, in the last series 1000 g thermite and 4 tubes were used.

In most experiments a high-speed camera was used to observe the flow and to determine the penetration as a function of time. Some experimental details are shown in the photos of Fig. 6 and 7.

2.3 Results

Series "1 tube"

One 4 mm i. d. tube was inserted down into the iron in the 3 experiments of this series. In Fig. 2 - 4 the penetration as a function of time (from the camera) and the final "post mortem" penetration from visual inspection is shown. The error in penetration depth deduced from the film is ≤ 2 cm.

For experiments 82/11/23-1 and -2 all controlled parameters were equal. Therefore it is very satisfactory, that the penetration depths are very similar (76 and 81 cm). The iron frozen in the tubes forms a compact slug. This finding is in contradiction with the impression from the film of downward moving in the lower part of the tube after blockage

in test 82/11/23-1. There is another interesting phenomena observed with all iron tests: Whereas the surface of the front part of the iron penetrated in the tube is dark, the back is bright (Fig. 2, 3). The dark/bright front moves upward with a velocity which is smaller than that of the leading edge. During movement the front is very sharp, after blockage it gets diffuse. Our explanation for this phenomena is the following: Initially a crust is formed at the cold wall. During the flow, the wall, which is essentially not cooled from outside, is heated up and the crust remelts.

Whereas in all other tests the tube inlet was open and the pressure was applied gradually after dip in, in test 82/11/23-3 (Fig. 4) the pressure was applied before dip in and the inlet was closed by a 0.1 mm Al foil, which melts at dip in. This change in experimental procedure has a strong influence on the type of flow: Whereas in all other tests the flow consists essentially of one plug, in 82/11/23-3 first some droplets and then several, separated plugs enter the tube (In previous studies with steel tubes and the same procedure as in 82/11/23-3 the melt frozen in the tube also consisted of many droplets and several plugs). For comparison with theoretical models the single plug flow is certainly more appropriate. Therefore the smooth pressurization after dip in was chosen for all other tests.

Series "3 tubes"

Three tubes (4 mm i. d.) were dipped at the same time into the same melt (680 g thermite). Therefore a thorough check of the reproducibility is possible. Important details of the tests of this series are summarized in Tab. 2. Dip in was at 23s, pressurization began 23.43 s after ignition. The time-dependance of the applied pressure difference is shown in Fig. 8, the melt temperature measured with the quartz glass-sealed W3Re/W25Re thermocouple in Fig. 9. The melt starts to flow when the pressure is applied (23.42 s) and the flow lasts about 1.5 s. The temperature 24 s after

ignition was therefore chosen to be representative for the inflowing melt and was determined by extrapolation of the measured thermocouple data (Fig. 9). The thermocouple needs some seconds to reach an asymptotic value and generally, about 10 s later, the thermocouples fail.

For each test a figure has been prepared (Fig. 10 - 16 and 19 - 28). These figures contain the pressure and, if available, the penetration as a function of time. In addition, the structure of the frozen material in the different tubes from post mortem visual inspection is shown on the right side. For each tube the inner diameter (i. d.), the distance of the inlet to the crucible bottom after dip in and the type of material (oxide: black, iron: yellow) is indicated. The position of the thermocouple, the environment (oxide or iron) and the extrapolated temperature during flow is also given if available.

Firstly from Tab. 2 it can be seen that the melt temperature did not differ much from test to test (maximum 2040, minimum 1870 °C). As well be shown later, these small variation in melt temperature have practical no effect on the penetration depth.

In the first three tests (83/2/16-1, /21-1, /22-1; Fig. 10 - 12) oxide flowed as one plug into the tubes. The reproducibility of the penetration depth is very satisfactory. In each test, the value for each individual tube is within about ± 5 cm (i. e. within ± 6 %) equal to the average of the three tubes. The maximum deviation between the values for two individual tubes of the same test amounts to about 16 %. In test 82/2/15-1 (Fig. 10) the pressure rise is steeper than in the other two tests (see Fig. 8) and this seems to cause a somewhat larger penetration depth. Two observations which were generally found with oxide melts should be mentioned. Firstly, the film shows that the leading edge (≈ 1 cm) is much brighter (i. e. hotter) than the surface which is in contact with the tube wall. This indicates that the surface at the head is continuously renewed

and therefore contains always hot liquid material. The post mortem inspection showed that in the upper part of the slug the central region (diameter some tenths of a mm) was either empty (central channel) or had a structure different from the outer regions. The diameter of this central region seems to decrease from top to bottom (inlet) and no such structure is found in the lower (10 - 20 cm) part. It is assumed that this structure is caused by the higher density of the solid compared to that of the liquid oxide. Plugging obviously occurs near the inlet. The shrinkage upon freezing than causes the central channel or the formation of a different structure in the upper part of the frozen slug (Fig. 10). Test 83/2/22-1 (Fig. 12) was the first of this series where the high speed 16 mm camera was used. No time marker was used on the film. The penetration versus time evaluated from the film was therefore correlated with the pressure signal by assuming that the flow starts when the pressure is applied (23.42 s after ignition). The final penetration deduced from the film is in excellent agreement with post mortem inspection. The flow lasts about 2 s. The velocity of the leading edge decreases continuously from an initial value of about 70 cm/s.

In test 83/2/23-1 (Fig. 13) the inlet of tube 1 and 2 were in the iron but near the interface. Therefore iron is followed by oxide. The flow in these tubes lasts only about 1.4 s, whereas the oxide flow in tube 3 lasts, as in the previous tests, about 2 s. As in the series 1 tests with iron, a dark/bright front, attributed to remelting of the crust, is observed.

In test 83/2/24-1 (Fig. 14) oxide flow (tube 3) starts before iron flow, nevertheless blockage occurs first in iron. In tube 2, where flow started latest, the flow velocity is very high, evidently because the pressure difference is already high at flow start. The penetration depths for the two iron filled tubes are in satisfactory agreement. In the upper part, the surface of the iron plug is rough, whereas in the lower part it is very even. This different surface structure seems to be correlated with the dark/bright front observed in the film.

Near the inlet, the iron plugs are covered with a thin oxide crust. This is caused by the small amount of oxide melt which enters the tube on its way down to the iron melt.

In test 82/2/25-1 (Fig. 15) the tubes were dipped into the oxide but just below the surface. This test was intended to simulate the conditions of the TRAN experiments /4/, where, because of the limited volume, the melt generally formed a crust in the tube. Only very few oxide entered tube 3, which was nearest to the surface. First some droplets enter the tube and the remaining oxide is deposited as a crust on the tube wall. Because now there is a connection between the vacuum chamber and the atmosphere, the pressure difference breaks down and therefore the penetration depths in tube 1 and 2 are small. Especially in this test, but also in some other experiments with oxide, the oxide near the tube wall is not so dark as usually, indicating probably beginning of quartz glass melting.

In test 83/2/25-2 (Fig. 16) the pressure gradient (Fig. 8) has been reduced as compared to the previous tests. As expected, the penetration depths are smaller. Unfortunately, the inlet of the tubes was near to the iron interface, therefore some iron droplets were mixed into the oxide.

Series "4 tubes"

Four quartz glass tubes were dipped at the same time into the same melt (1000 g thermite). The main goal was the determination of the penetration depth as a function of the tube inner diameter. The tests are summarized in table 3. As in series "3 tubes" dip in was at 23 s, pressurization began 23.42 s after ignition. The pressure difference and the thermocouple signals are shown in Fig. 17 and 18, respectively.

Again the reproducibility is very satisfactory (Tab. 3). With a few exceptions one single plug is flowing into the tubes. Again a central channel is found in the upper part of the oxide slug. Similar as in the previous tests a dark/bright front was observed with the iron melts, but it was not evaluated in this series. The iron plugs are in the lower part again covered by a thin oxide crust.

In the first three tests (Tab. 3) 4 mm i. d. tubes were dipped into the oxide. Test 83/3/24-1 (Fig. 19) gives a good impression of the reproducibility. In test 83/4/14-1 (Fig. 20) some iron is intermixed in tube 2 and 3. This seems to reduce the penetration depth.

Test 83/4/21-1 (Fig. 21) was the only where a different type of thermite (type IRE) was used. This thermite has been mixed from pure Al and iron oxide in the laboratory. The density is smaller and it reacts more violent than the normally used thermite. Therefore only 600 g could be used and a remarkable percentage was lost during the reaction (no losses occurred with the normally used thermite). Because of the small melt volume, the melt temperature was low (1900 °C) and a break-through with continuous crust formation (TRAN type) occurred in tube 2. The low temperature and the decreased pressure difference (Fig. 17) caused by break-through results in comparable small penetration depths of about 60 cm.

In the next four tests (83/4/21-2, /22-1, /22-2, /25-1; Fig. 22 - 25) the dependance of penetration depth versus channel diameter for oxide was studied systematically, by dipping into the same melt tubes with different diameters. The increase of flowing time and penetration depth with increasing channel diameter is clearly visible. The penetration depths for the same channel diameter are in very good agreement.

The last three tests (83/4/26-1, /26-2, /27-1, Fig. 26 - 28) served mainly to study the dependance of penetration depth versus channel diameter for iron. Some tubes were inserted

in the oxide to allow cross checks with previous data. Similar as for oxide, the iron tests demonstrate clearly the increase in flow time and penetration depth with channel diameter. Surprisingly, for the channel diameters investigated here (4, 3 and 2 mm), the penetration depth for iron is very nearly equal to that for oxide. For the iron tests again the oxide crust in the lower part and different surface roughnesses are observed. The post mortem inspection of these last three tests revealed some deformation (to an elliptical shape) and melting (some quartz glass is embedded in the iron plugs, Fig. 26 and 27) of the tube inlet section. The influence of this effect has to be studied in further experiments.

3. Discussion of results

Firstly some qualitative results from observations of the films and from post mortem inspection are summarized:

Oxide: The leading edge is very bright, indicating that this is the only part where liquid material is visible. The central region in the upper part of the plug has a different structure indicating that plugging occurs near the tube entrance. Occasionally, the oxide layer adjacent to the wall looks different indicating beginning of wall melting.

Iron: A sharp dark/bright front is observed, indicating remelting of the crust in the lower part of the tube. From this it may be concluded that, in contrast to oxide, plugging occurs near the leading edge of the flow. Because the tubes have to pass the oxide, a small amount of oxide enters the tube and plates out as thin crust in the lower part of the tube.

Although this was not the aim of this study, some information on the dependance of penetration depth on melt temperature and pressure gradient is contained in the data. In Fig. 29,

the oxide data of series "3 tubes" for a channel diameter of 4 mm and nearly equal initial pressure gradient $\Delta p/\Delta t$ demonstrate, that the penetration depth increases only slightly with the melt temperature. The data in Fig. 30, again for oxide and a 4 mm channel diameter, show a definite, but moderate increase of the penetration depth with the initial pressure gradient (i. e. velocity).

The most interesting results, referring to the dependence of penetration depth on channel diameter, are contained in Fig. 31. In the left part only those data have been selected, where at least two tubes were dipped in the same and the same type (oxide or iron) of melt. For these pairs or triples of data, the melt temperature and pressure gradient were identically, therefore the channel diameter was the only parameter which was different. A careful look at these data shows, that the scatter (under identical boundary conditions) of about ± 5 cm is comparable or even larger than the effects of melt temperature and pressure gradient. Therefore in the right part of Fig. 31 all data (except 83/2/16-1: very high $\Delta p/\Delta t$ and 83/2/25-2: very low $\Delta p/\Delta t$) have been summarized. Under our experimental conditions and for channel diameters between 2 and 4 mm, the penetration depth of iron and oxide is equal and it increases strongly with the channel diameter.

Using the material properties of Tab. 4, the experimental penetration depths have been compared with an experimental correlation and a conduction model (Tab. 5) given by Cheung and Baker /5/. What concerns the material properties, the melting points as determined in this work has been taken. The other data for iron has been assumed to be equal to that for stainless steel /6/. For oxide, $Pr \approx 1$ and $\alpha_m/\alpha_s \approx 1$ (the symbols are defined in Tab. 4) has been assumed and the viscosity μ was chosen to be about equal to that of iron and UO_2 /6/.

The calculated penetration depths are given in Tab. 5 and in Fig. 31. The same factor $(1 + \gamma \frac{c_m(T_o - T_f)}{h})$, as proposed in the empirical correlation, was used for the conduction model to take into account the superheat of the melt (T_o is the measured tem-

perature of the melt at the tube inlet). The tube walls were initially at room temperature and essentially adiabatic. Therefore a reasonable assumption for the wall temperature is $T_w \approx T_f/2$. The experimentally determined flow velocities v were used to calculate the Reynolds numbers.

Whereas for the oxide melts the superheat increases the penetration depth by only 16 %, for iron the increase is more than a factor two.

Although the empirical correlation underpredicts the penetration depth by about a factor two (Fig. 31), it is insofar in agreement with the experiments, as it predicts comparable penetration depths for oxide and iron. The conduction model is for oxide in reasonable agreement with the experiments, although the dependence on the channel diameter D is too strong. For iron there is a severe underprediction of the conduction model, indicating that the influence of the material properties is not adequately taken into account. More sophisticated models - like PLUGM /7/ - are required for the description of fuel freezing and the experimental data presented here provide a good basis to check these models.

Acknowledgement

Thanks are due to M. Bober, I. Schub, G. Schumacher, J. Singer and K. Wagner for the determination of the melting points and the SEM analysis.

Literature

- /1/ G. A. Greene, J. U. Berry
"Freezing of Multiphase Mixtures Flowing Downward in
Circular Tubes"
BNL-NUREG-28302 (1980)
- /2/ B. W. Spencer et al.
"Results of Fuel Freezing Tests with Simulated CRBR-type
Fuel Pins"
ANS Trans. 30 (1978) p. 446
- /3/ M. Amblard and G. Maurin
"An Approach of Molten fuel Relocation Problem: Fuel
Freezing"
ENS/ANS Int. Topical Meeting on Nuclear Power Reactor
Safety, Brussels, 1978
- /4/ D. A. McArthur, N. Haydn and S. F. Duliere
"The TRAN Experiment Series in the Sandia ACRR facility"
Int. Topical Meeting on Liquid Metal Fast Breeder Reactor
Safety and Related Design and Operational Aspects, Lyon, 1982
- /5/ F. B. Cheung and L. Baker
"Transient Freezing of Liquids in Tube flow"
Nucl. Sci. Eng. 60 (1976) 1 - 9
- /6/ L. Leibowitz et al.
"Properties of LMFBR Safety Analysis"
ANL-CEN-RSD-76-1 (1976)
- /7/ M. Pilch, P. K. Mast
"PLUGM, A Coupled Thermal-Hydraulic Computer Model for
Freezing Melt Flow in a Channel"
NUREG/CR-3190 (1983)

Tab. 1 Results SEM analysis

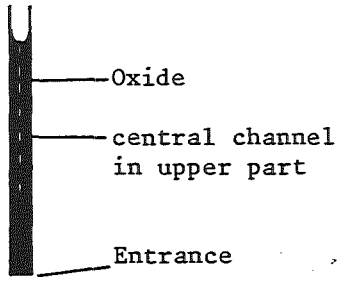
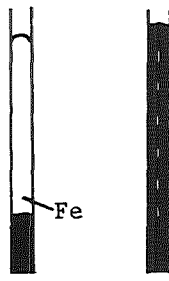
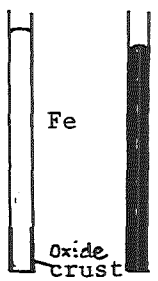
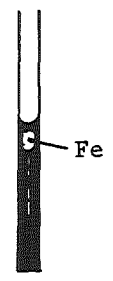
Sample	At %							
	Al	Si	Fe	K				
Crucible, Series "3 quartz glass tubes"	19	72	-	9				
Crucible, Series "4 quartz glass tubes"	27	60	-	13				
Series "4 tubes"	Test 83/4/21-2	Oxide in tube		76	10	14	-	
Thermite 10/R70-SSH (19.05.82)	Test 83/4/22-2	Oxide in tube	Sample 1		79	10	11	-
				74	11	15	-	
				79	7	14	-	
		Sample 2		75	10	15	-	
				74	11	15	-	
		Oxide in crucible	Position 1	2	44	22	34	-
2	54			30	16	-		
Series "4 tubes"		Oxide in tube	2	77	22	.35	-	
Thermite IRE Test 83/4/21-1		Oxide in crucible	Position 1	50	38	12	-	
			2	61	35	3.4	-	

Tab. 2 3 quartz glass tubes, inner diameter 4 mm, wall thickness 1 mm, length 100 cm
680 g thermite, type 10/R 70-SSH (19.05.82)

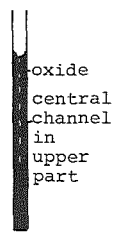
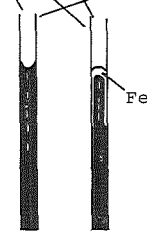
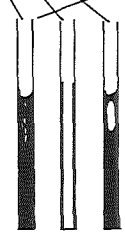
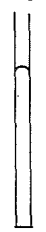
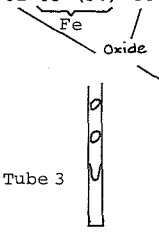
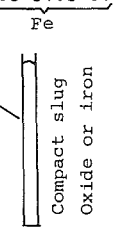
Crucible inner, upper ϕ 78 mm

Time program: Ignition 0 s, dip in 23 s, pressure 23.42 s

Temp. meas.: W3Re/W25Re TC in quartz glass; Camera 16 mm (480 f/s)

	83/2/16-1	83/2/21-1	83/2/22-1	83/2/23-1	83/2/24-1	"TRAN" 83/2/25-1	83/2/25-2		
Initial $\Delta p/\Delta t$ (bar/s)	1.6	.65	.70	.64	.78	-	.59		
Melt Type T($^{\circ}$ C), 24 s	Al_2O_3 1870 \pm 20, Al_2O_3	Al_2O_3 2040 \pm 20, Al_2O_3	Al_2O_3 2000 \pm 20, Al_2O_3	Fe/ Al_2O_3 2010 \pm 30, Fe/ Al_2O_3	Fe/ Al_2O_3 1950 \pm 20, Al_2O_3	Al_2O_3 1930 \pm 30, Al_2O_3	Al_2O_3 1960 \pm 20, Fe/ Al_2O_3		
Tube no.	1 2 3								
Penetration depth (cm)	84 92 96	75 77 89	70 76 70	73 72 78	86 73 72	15 13.5 14	57 45 56		
									
Average penetration depth (cm)	91 ± 5 7	80 ± 9 5	72 ± 4 2						

Tab. 3 4 quartz glass tubes, wall thickness 1 mm, length 100 cm
 1000 g thermite, type 10/R70-SSH (19.05.82)
 Crucible inner, upper \varnothing 85 mm
 Time program: Ignition 0 s, dip in 23 s, pressure 23.42 s
 Temp. meas.: W3Re/W25Re in quartz glass; Camera 16 mm (480 f/s)

	83/3/24-1	83/4/14-1	600 g thermite "IRE" 83/4/21-1	83/4/21-2	83/4/22-1	83/4/22-2	83/4/25-1	83/4/26-1	83/4/26-2	83/4/27-1
Init. $\Delta p/\Delta t$ (bar/s)	-	.88	.88	1.09	1.05	1.14	1.21	1.09	1.03	1.14
Melt Type T(°C), 24s	Al ₂ O ₃ -	Al ₂ O ₃ 2100±20, Al ₂ O ₃	Al ₂ O ₃ 1900±40, Al ₂ O ₃	Al ₂ O ₃ -	Al ₂ O ₃ 2030±20, Al ₂ O ₃	Al ₂ O ₃ 2000±20, Al ₂ O ₃	Al ₂ O ₃ 2030±20, Al ₂ O ₃	Fe 2140±20, Fe	Fe/Al ₂ O ₃ 2110±20, Fe	Fe/Al ₂ O ₃ 2180±40, Fe
Tube no. Inner \varnothing (mm)	1 2 3 4 4	1 2 3 4 4	1 2 3 4 4	1 2 3 4 4 3	1 2 3 4 4 3	1 2 3 4 4 2	1 2 3 4 2 4 3	1 2 3 4 2 4 3	1 2 3 4 4 3	1 2 3 4 2 3 4
Penetration (cm)	89 79 92 84 	79 69 62 76 	57 69 62 60 	84.5 86.5 48 42.5 	87 88 65.5 53 	92 91 21 19	22.5 85 53.5 66	25 84 58 46 	82 83 (31) 44 	28.5 51.5 81 82 
Average penetration depth (cm)	86 ± 7	77.5 ± 1.5 (tube 1, 4)	-	85.5 ± 1 45 ± 3	87.5 ± 1 59 ± 6	91.5 ± 1 20 ± 1	- 60 ± 6	- 52 ± 6	-	-

Tab. 4 Material properties

	Fe (SS 304 [6])	Oxide
Melting point T_f ($^{\circ}\text{C}$)	1510 (own meas.)	1830 (own meas.)
Heat of fusion h (J/g)	266	1073*
Specific heat c (J/g $^{\circ}\text{C}$)	solid molten	solid molten
	.60 (700 $^{\circ}\text{C}$) .79	1.2 (700 $^{\circ}\text{C}$)* 1.4 (2200 $^{\circ}\text{C}$)*
Thermal diffu- sivity α (cm 2 /s)	solid molten	solid molten
	.053 (700 $^{\circ}\text{C}$) .032	$\frac{\alpha_m}{\alpha_s} \approx 1$ (assumed)
Density ρ (g/cm 3)	solid molten	solid molten
	7.6 (700 $^{\circ}\text{C}$) 6.9	4.0*
Viscosity μ (g/cms) ν (cm 2 /s)	μ (g/cms) ν (cm 2 /s)	μ (g/cms) ν (cm 2 /s)
	.040 (1700 $^{\circ}\text{C}$) .0059 (1700 $^{\circ}\text{C}$)	.04 (assumed) .01
$Pr = \left(\frac{\nu}{\alpha}\right)_m$.18	1 (assumed)

*S. Dorner, G. Schumacher, "Metall für die exotherme Reaktion mit Eisenoxid zur Simulation großer Kernschmelzen", July 1977, unpublished

Tab. 5 Calculated penetration depth Z

Cheung and Baker /5/ Experimental correlation $Z/D = KRe^{3/4} \left(\frac{h}{c_s(T_f - T_w)} \right)^{1/3} \left(1 + \gamma \frac{c_m(T_o - T_f)}{h} \right)$; $K = .23 Pr^{1/2} \left(\frac{\alpha_m}{\alpha_s} \right)^{1/9}$

$\gamma = 0.7$

$Pr = \nu/\alpha$

$Re = vD/\nu$

T_o = initial temperature of melt

D = channel diameter

Conduction model $Z/D = \frac{1}{16} Re Pr \frac{\alpha_m}{\alpha_s} \frac{h}{c_s(T_f - T_w)}$

D (cm)	Iron								Oxide			
	v(cm/s)	Re	Penetration depth (cm)				v(cm/s)	Re	Penetration depth (cm)			
			Emp. Correlation $T_o = 2100^\circ C$		Conduction model $T_o = T_f \quad T_o = 2100^\circ C$				Emp. corr. $T_o = 2000^\circ C$	Cond. model $T_o = 900^\circ C$		
			$T_w = 20^\circ$	$T_w = 800^\circ C$	$T_w = 20^\circ C$	$T_w = 800^\circ C$						
.4	110	7500	44.8	57.4	6.0	12.9	29.0	90	3600	48	99	
.3	90	4600	23.3	29.8	2.8	5.9	13.3	70	2100	24	43	
.2	75	2500	9.8	12.6	1.0	2.2	5.0	50	1000	9.2	12	

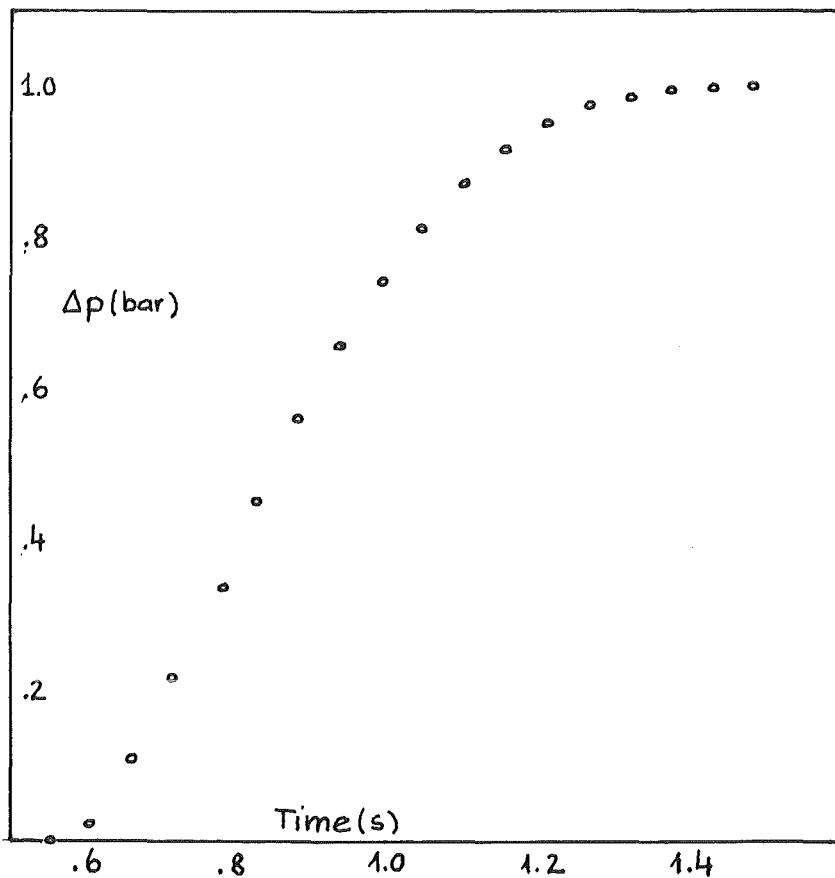


Fig. 1 Series "1 Tube"
Pressure in sphere above atmospheric
($\hat{=}$ pressure difference)

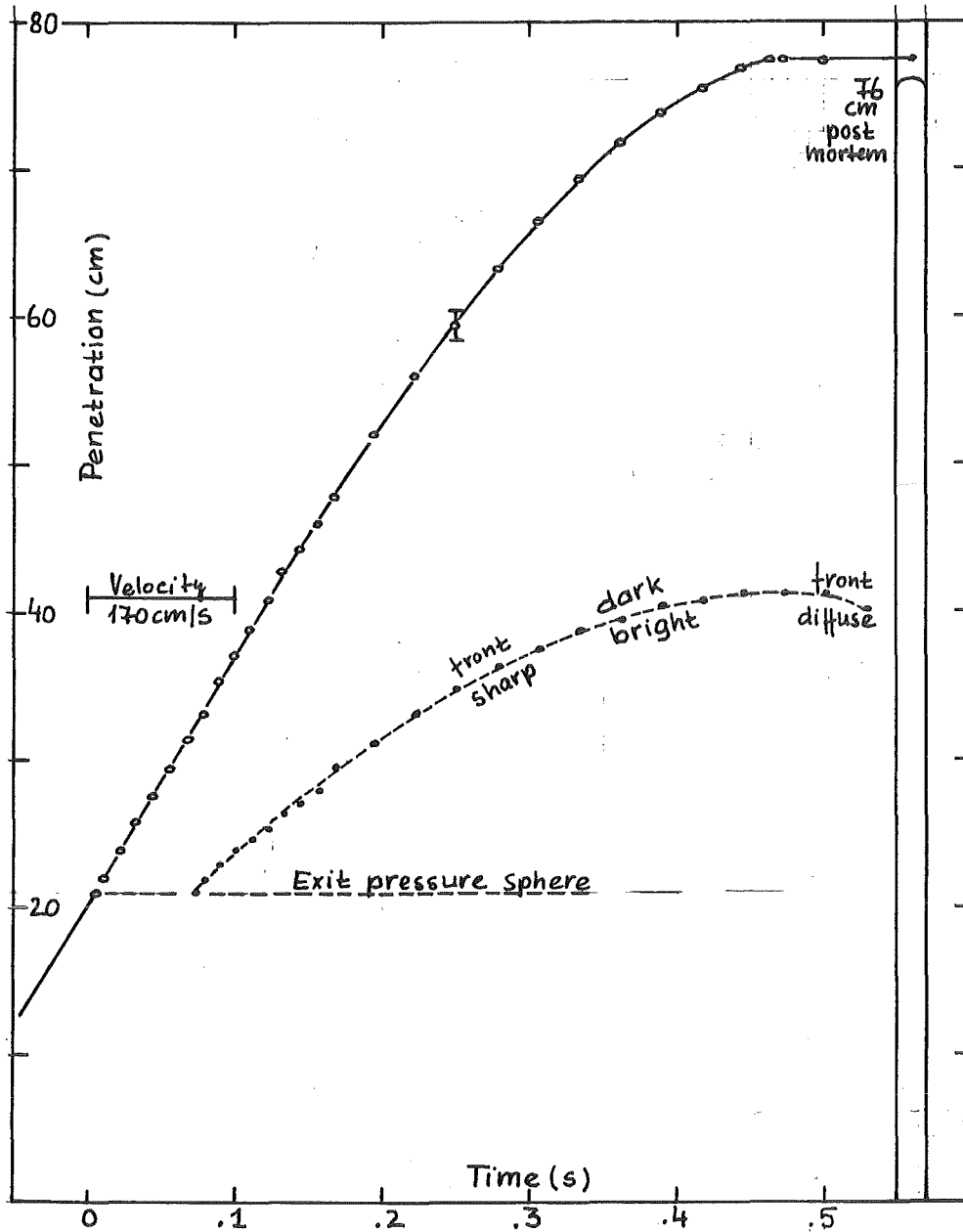


Fig. 2 Series "1 tube", pressure sphere, $\Delta p = 1$ bar
Test 82/11/23-1, tube: i. d. 4 mm, wall 1 mm, length 100 cm
350 g thermite; dip in ≈ 30 s, pressure ≈ 31 s after
ignition
Melt: Fe, estimated $T = 1800 \pm 100$ °C (32 s); Camera
Super 8 (180 f/s)

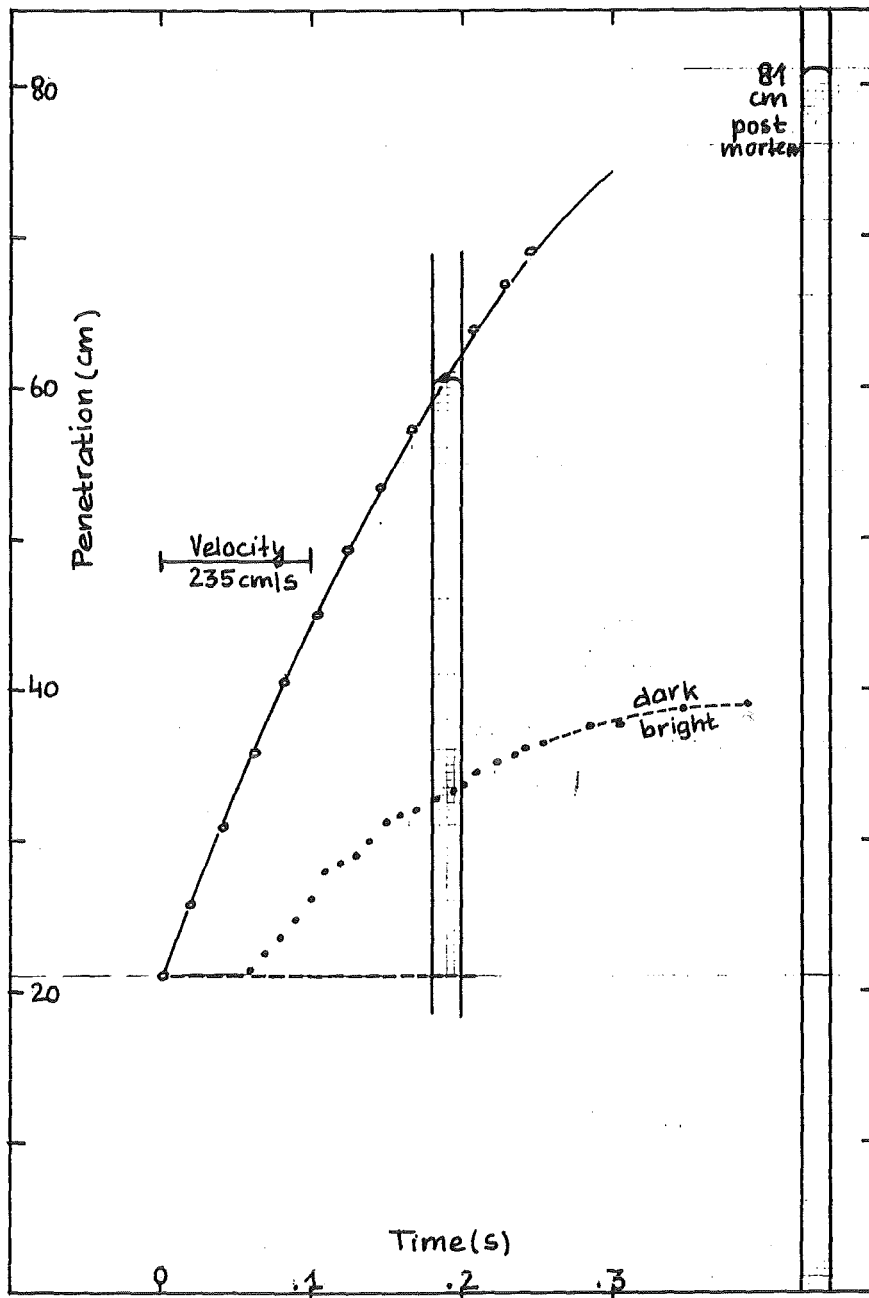


Fig. 3 Series "1 tube", pressure sphere, $\Delta p = 1$ bar
Test 82/11/23-2; tube: i. d. 4 mm, wall 1 mm, length 100 cm
350 g thermite; dip in ≈ 30 s, pressure ≈ 31 s after ignition
Melt: Fe, estimated $T = 1800 \pm 100$ °C (32 s);
Camera 16 mm (480 f/s)

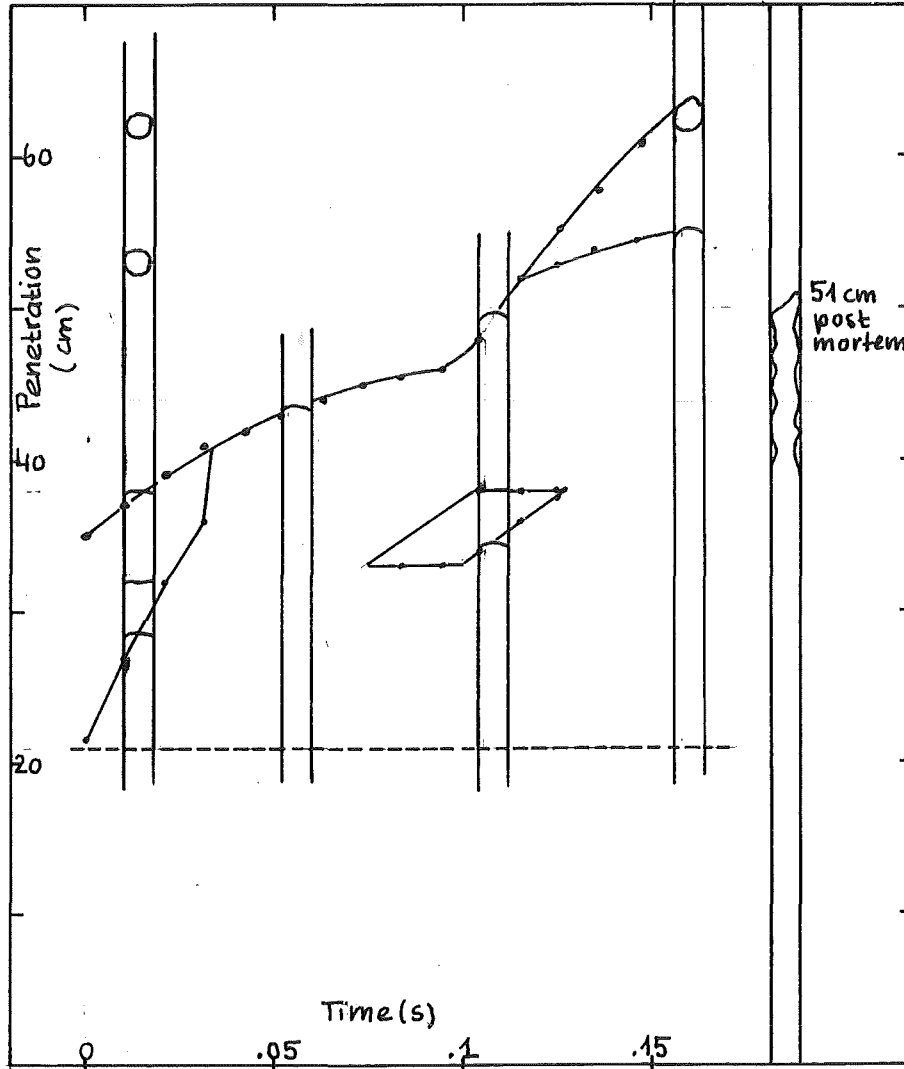


Fig. 4 Series "1 tube", pressure sphere, $\Delta p = 0.6$ bar
Test 82/11/23-3; tube: i. d. 4 mm, wall 1 mm, length 100 cm
350 g thermite; pressure before dip in (30 s after ignition);
Tube inlet closed by 0.1 mm Al foil
Melt: Fe, estimated $T = 1800 \pm 100$ °C (32 s);
Camera 16 mm (480 f/s)

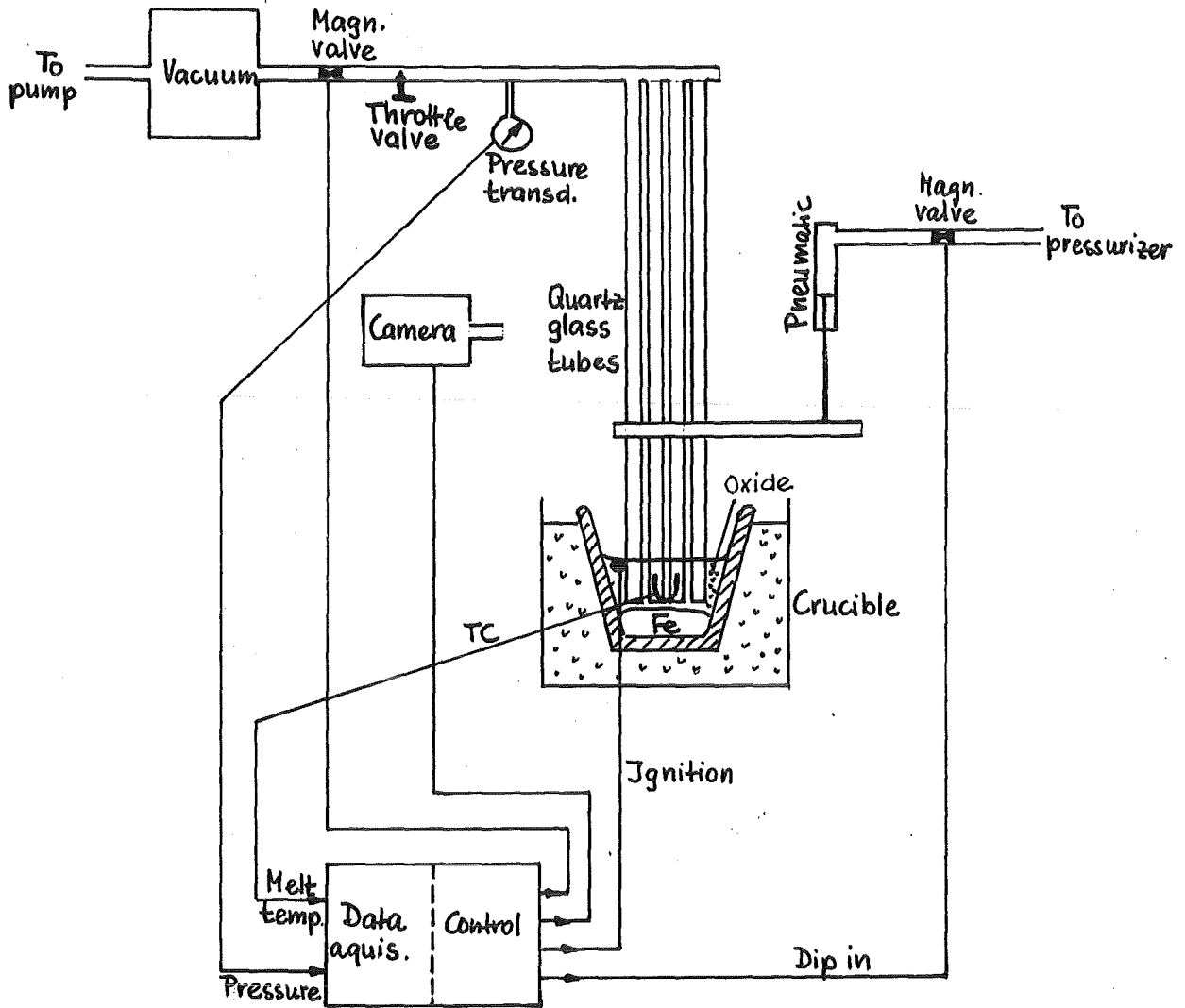


Fig. 5 Experimental setup for test with evacuated exit
(Series "3" and "4 tubes")

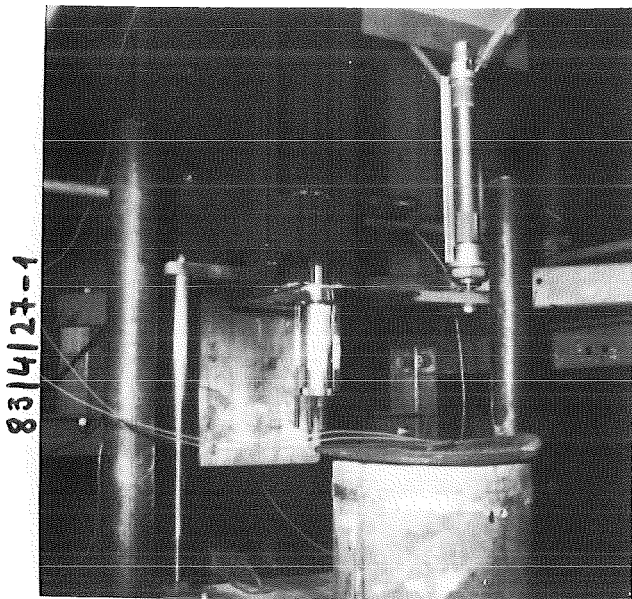
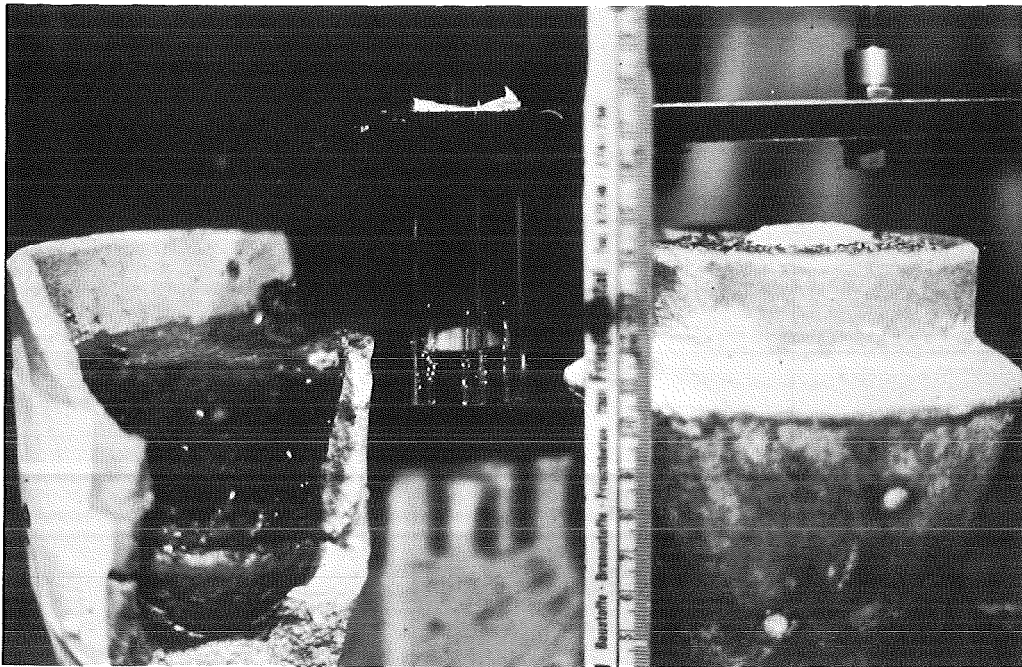


Fig. 6 Upper photo: Series "3 tubes", crucible before and after reaction, tube inlet and WRe thermocouple
Lower photos: Series "4 tubes",
Left: before test, crucible, tubes, pneumatic
Right: Oxide filled tubes after test

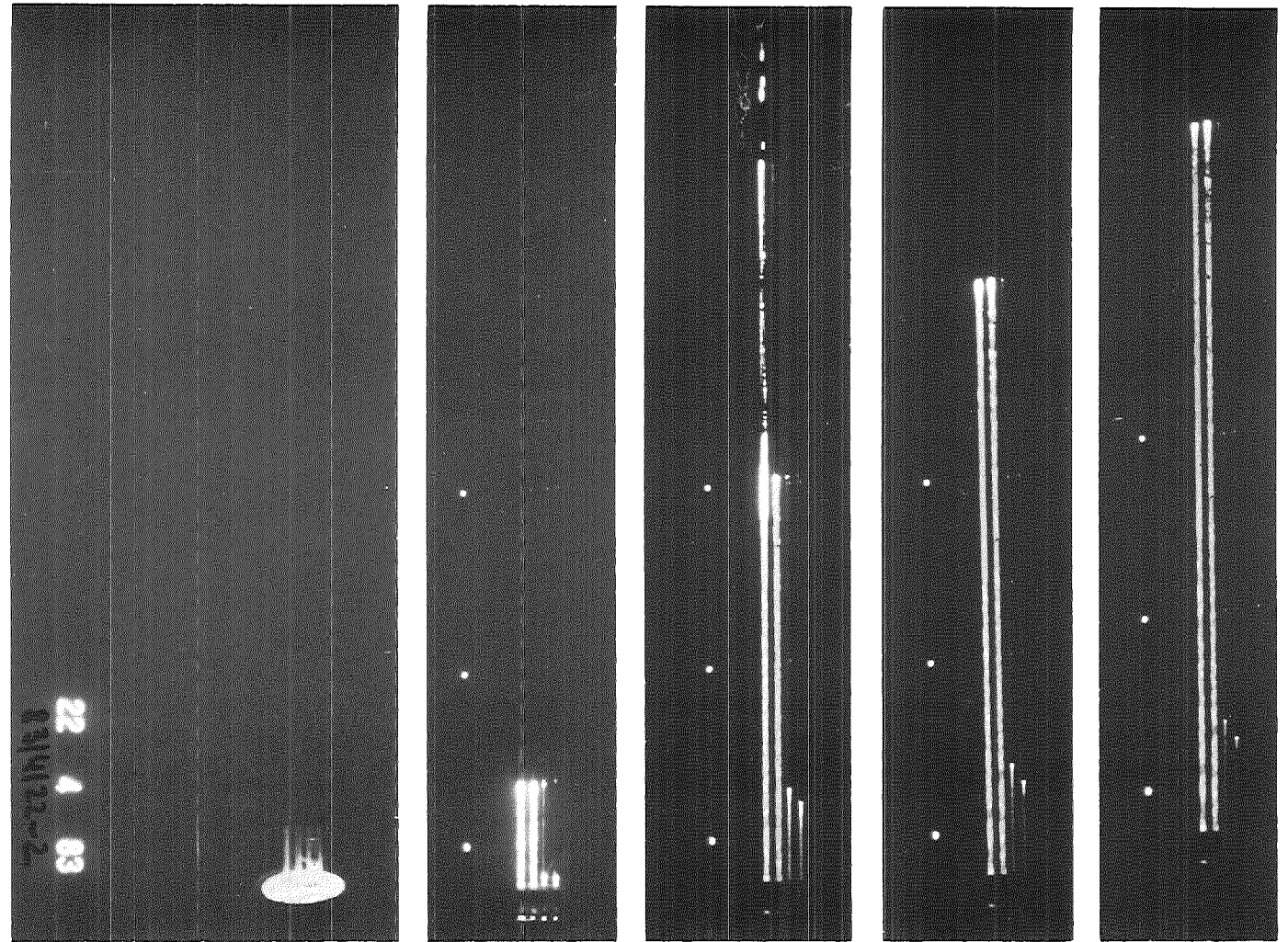
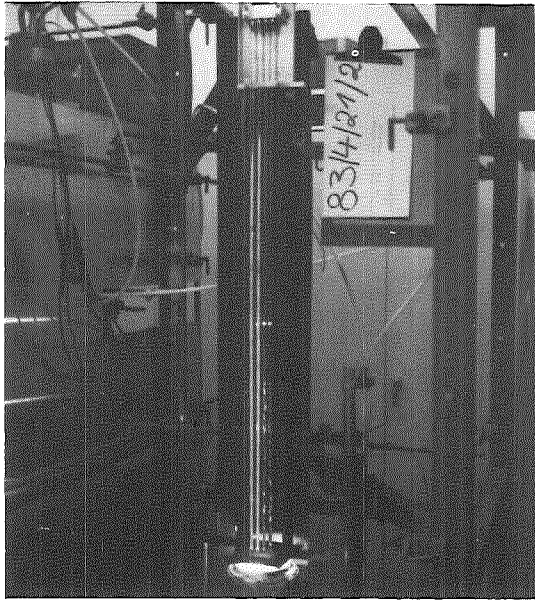


Fig. 7 Series "4 tubes"

Left: Test 83/4/21-2; glowing, oxide filled tubes

Right: Test 83/4/22-2; flowing oxide (hand camera 3.5 f/s)

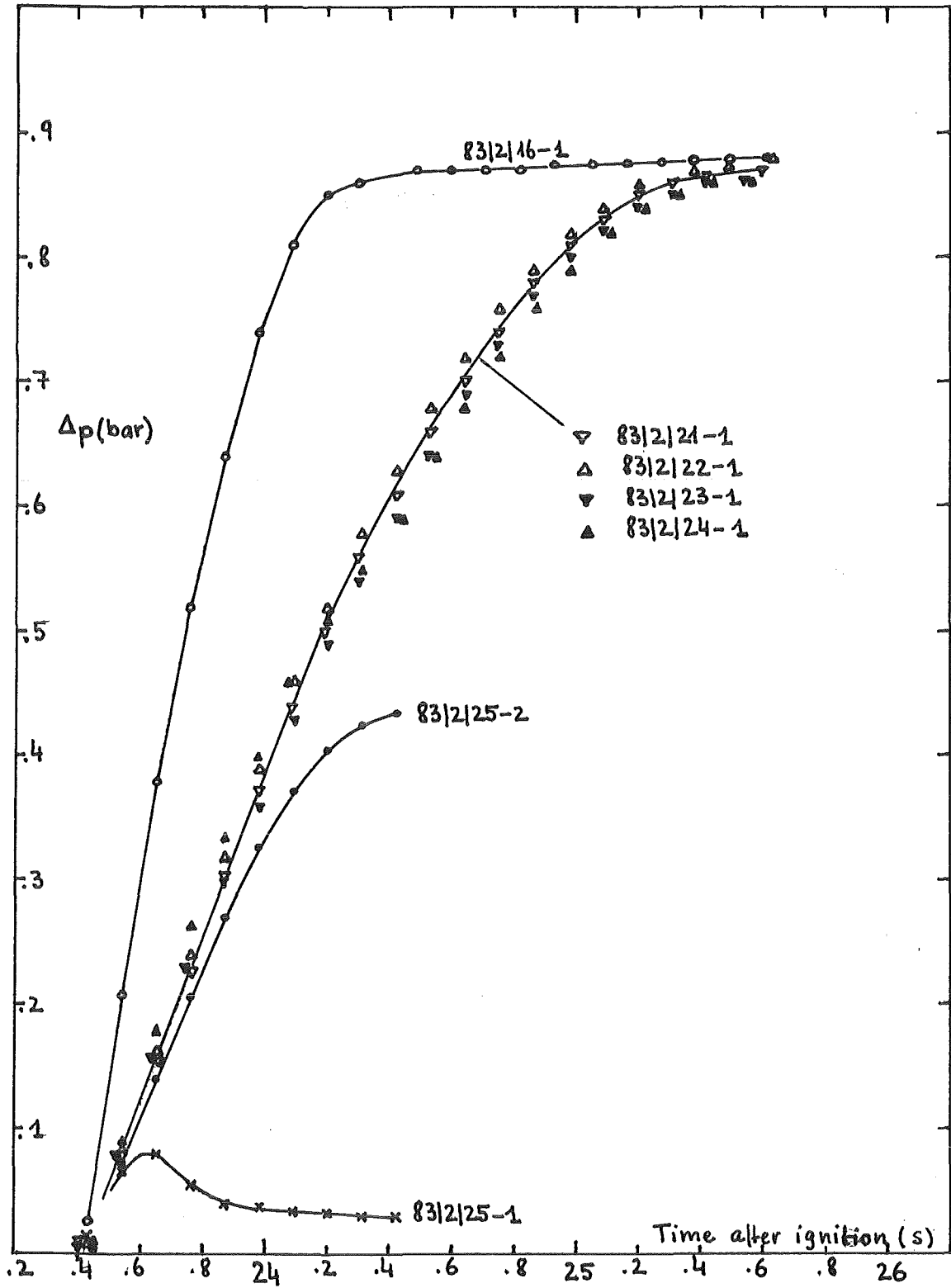


Fig. 8 Series "3 tubes", pressure difference

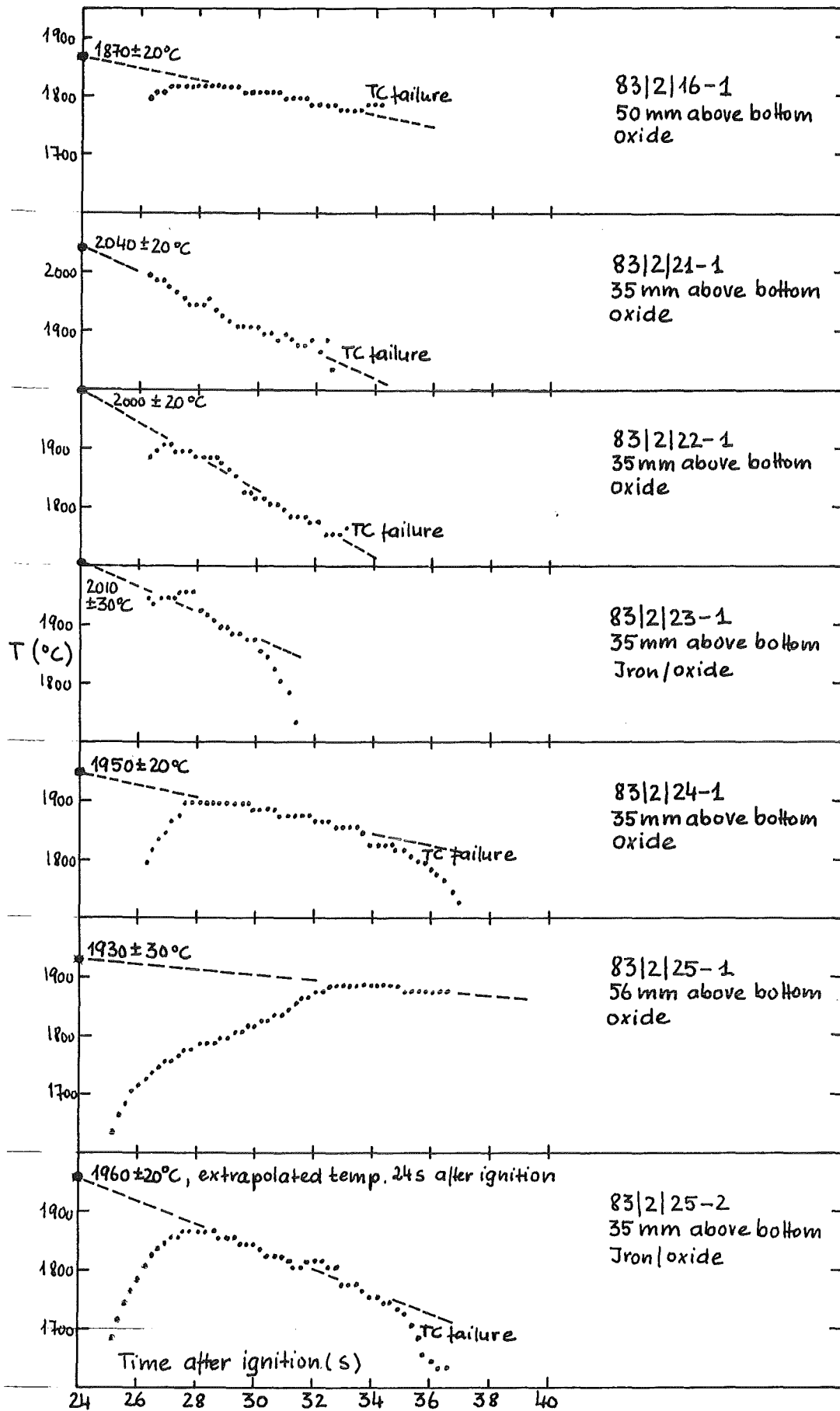


Fig. 9 Series "3 tubes", melt temperature measured with W3Re/W25Re thermocouples

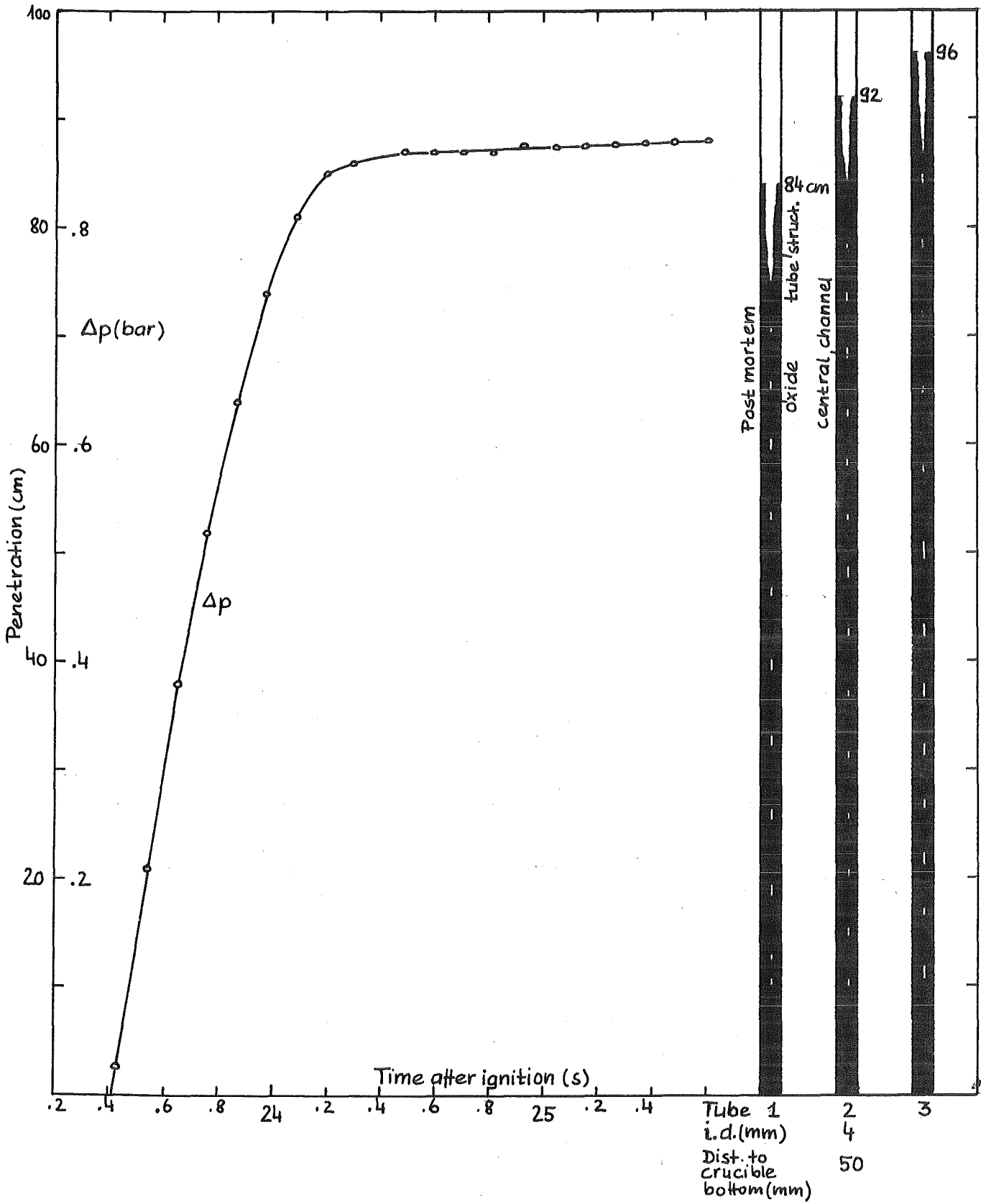


Fig. 10 Series "3 tubes", test 83/2/16-1
 Tubes: Wall 1 mm, length 100 cm; 680 g thermite
 Dip in 23 s after ignition
 Melt: Oxide, $T = 1870 \pm 20$ °C (24 s, 50 mm above bottom)
 High pressure difference

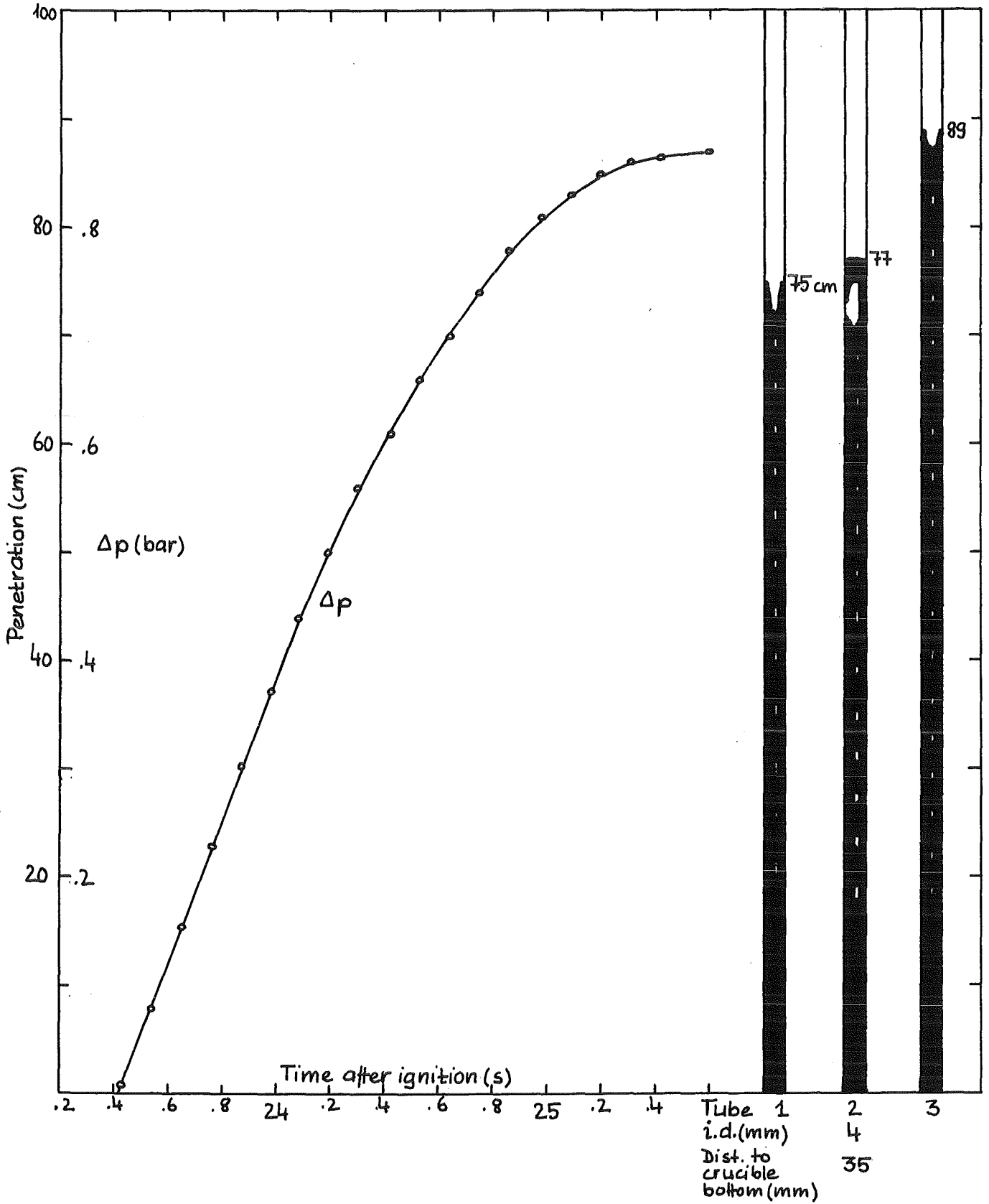


Fig. 11 Series "3 tubes", test 83/2/21-1
 Tubes: Wall 1 mm, length 100 cm; 680 g thermite
 Dip in 23 s after ignition
 Melt: Oxide, $T = 2040 \pm 20$ °C (24 s, 35 mm above bottom)

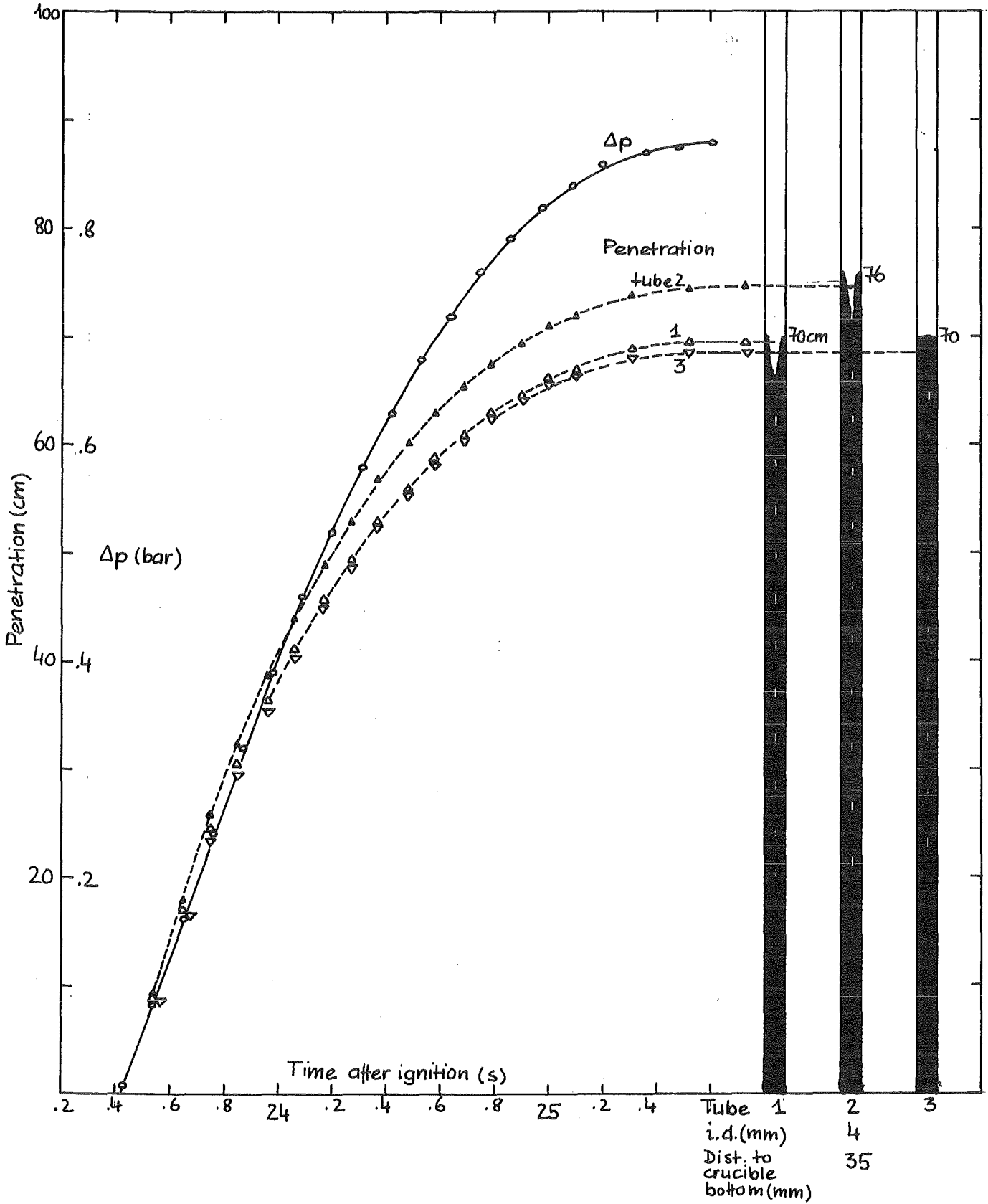


Fig. 12 Series "3 tubes", test 83/2/22-1
 Tubes: Wall 1 mm, length 100 cm; 680 g thermite
 Dip in 23 s after ignition
 Melt: Oxide, $T = 2000 \pm 20$ °C (24 s, 35 mm above bottom)

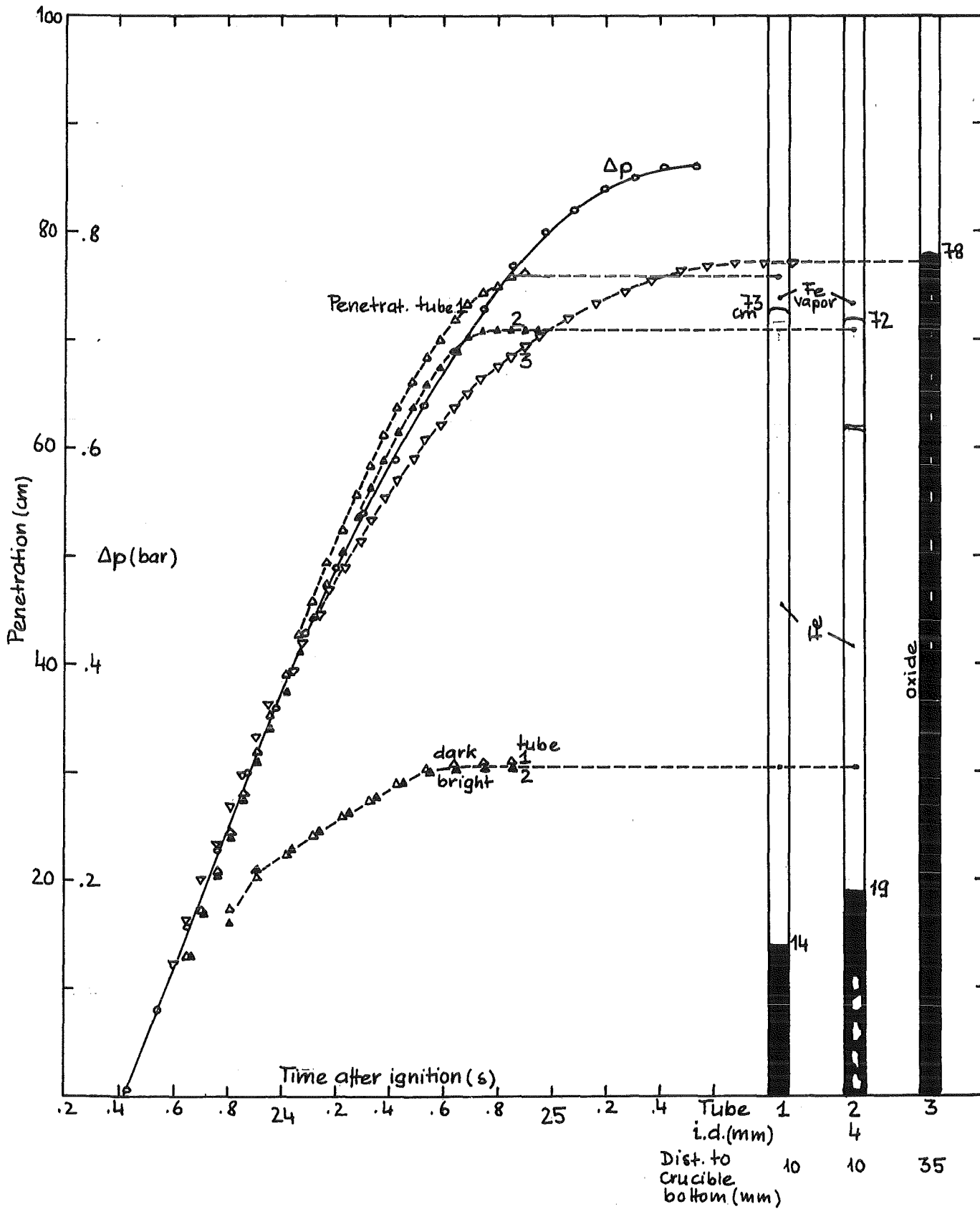


Fig. 13 Series "3 tubes", test 83/2/23-1
 Tubes: Wall 1 mm, length 100 cm; 680 g thermite
 Dip in 23 s after ignition
 Melt: Oxide, $T = 2010 \pm 30$ °C (24 s, 35 mm above bottom)
 Iron

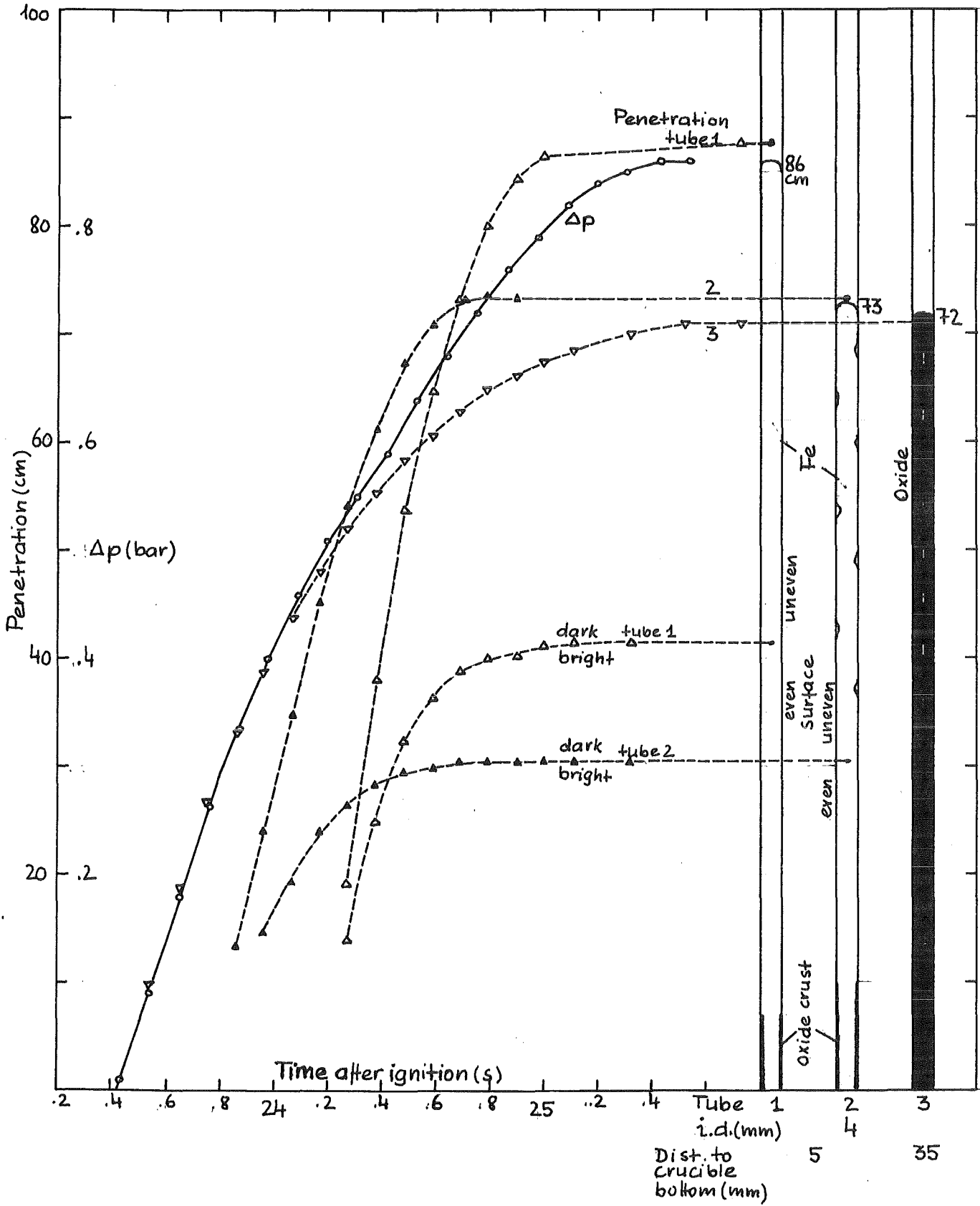


Fig. 14 Series "4 tubes", test 83/2/24-1
 Tubes: Wall 1 mm, length 100 cm; 680 g thermite
 Dip in 23 s after ignition
 Melt: Oxide, $T = 1950 \pm 20$ °C (24 s, 35 mm above bottom)
 Iron

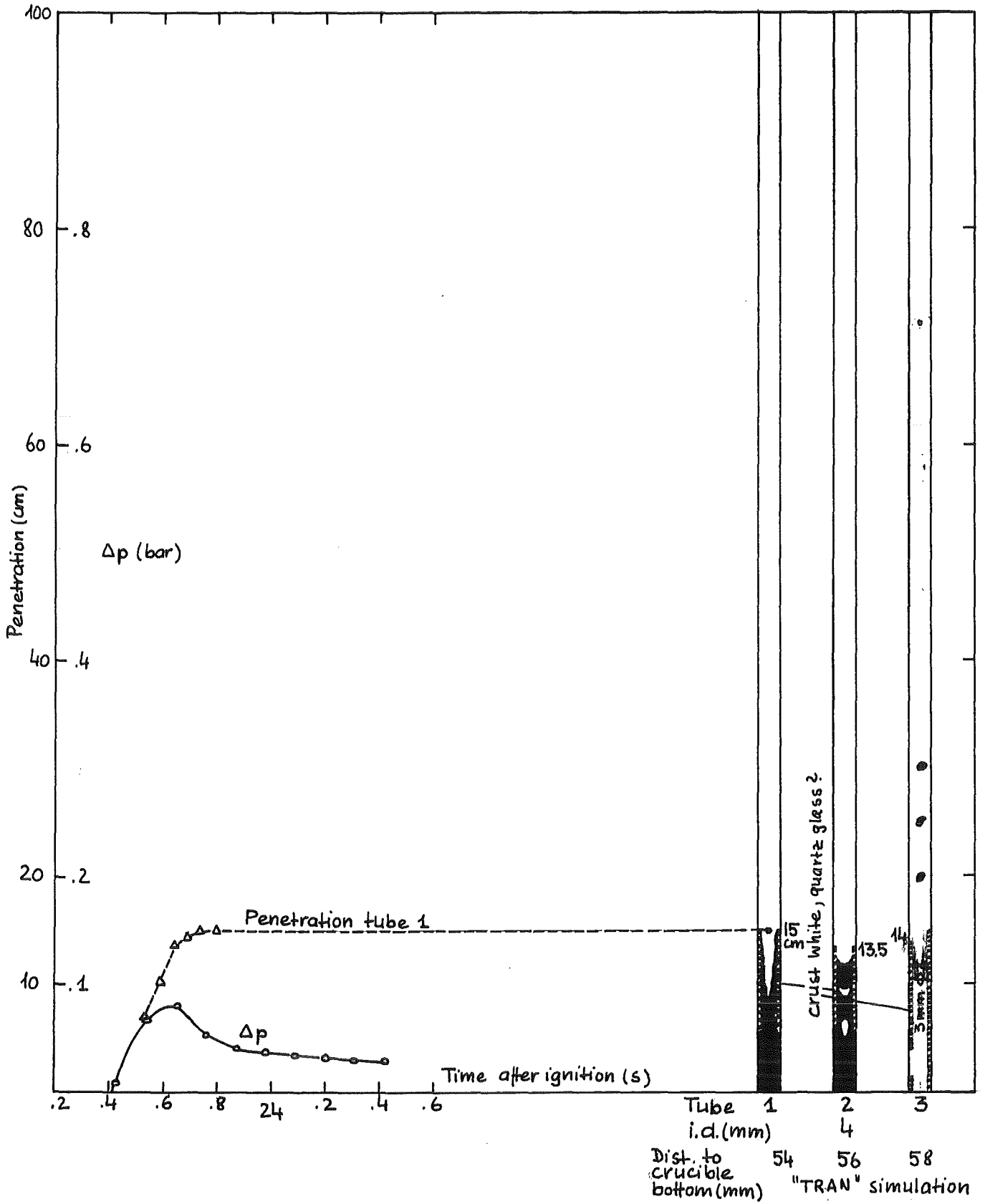


Fig. 15 Series "3 tubes", test 83/2/25-1
 Tubes: Wall 1 mm, length 100 cm; 680 g thermite
 Dip in 23 s after ignition
 Melt: Oxide, $T = 1930 \pm 30$ °C (24 s, 56 mm above bottom)
 TRAN simulation, white crust indicates quartz glass melting

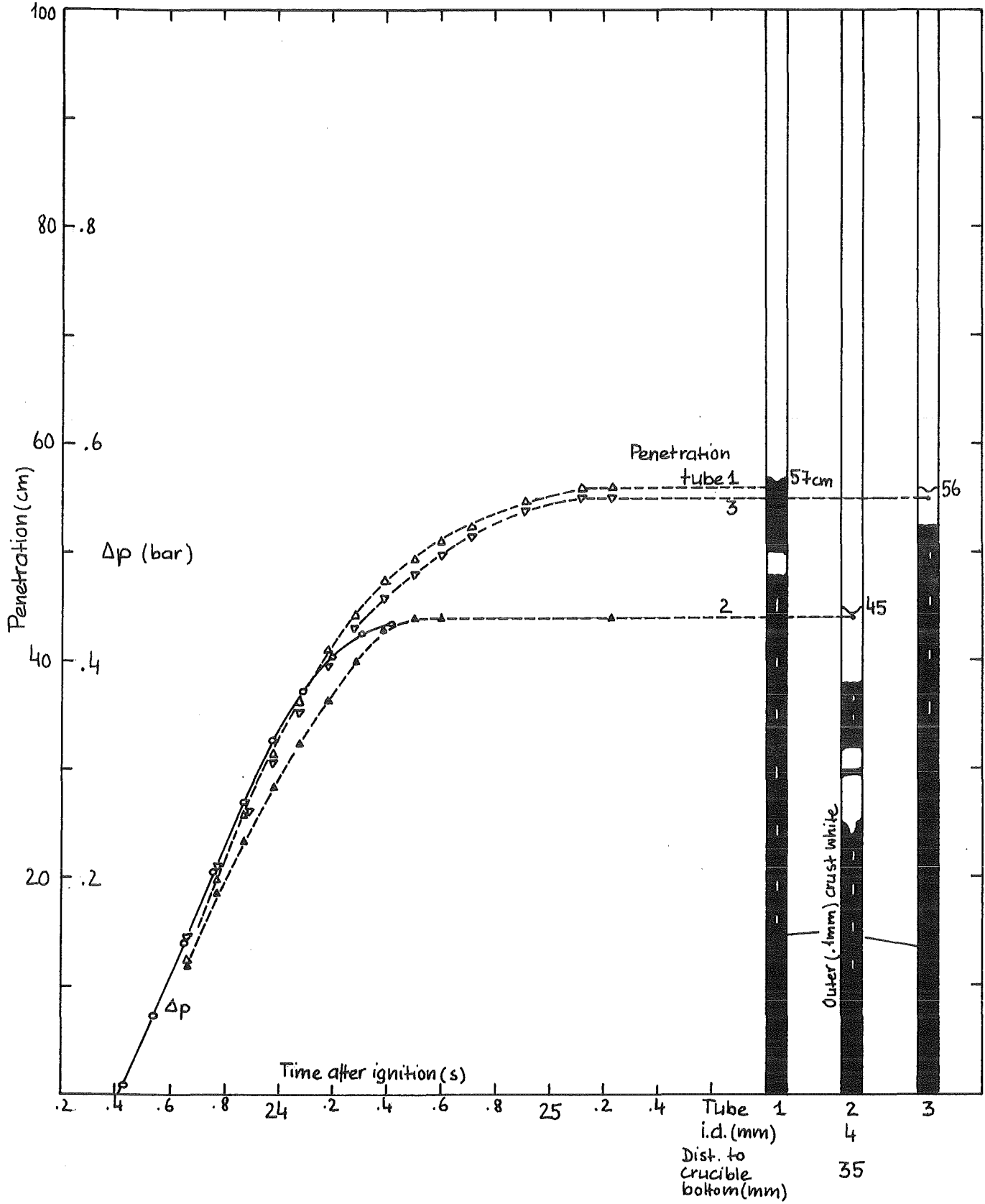


Fig. 16 Series "3 tubes", test 83/2/25-2
 Tubes: Wall 1 mm, length 100 cm; 680 g thermite
 Dip in 23 s after ignition
 Melt: Oxide (+ some iron), $T = 1960 \pm 20$ °C (24 s,
 35 mm above bottom)
 Low pressure difference

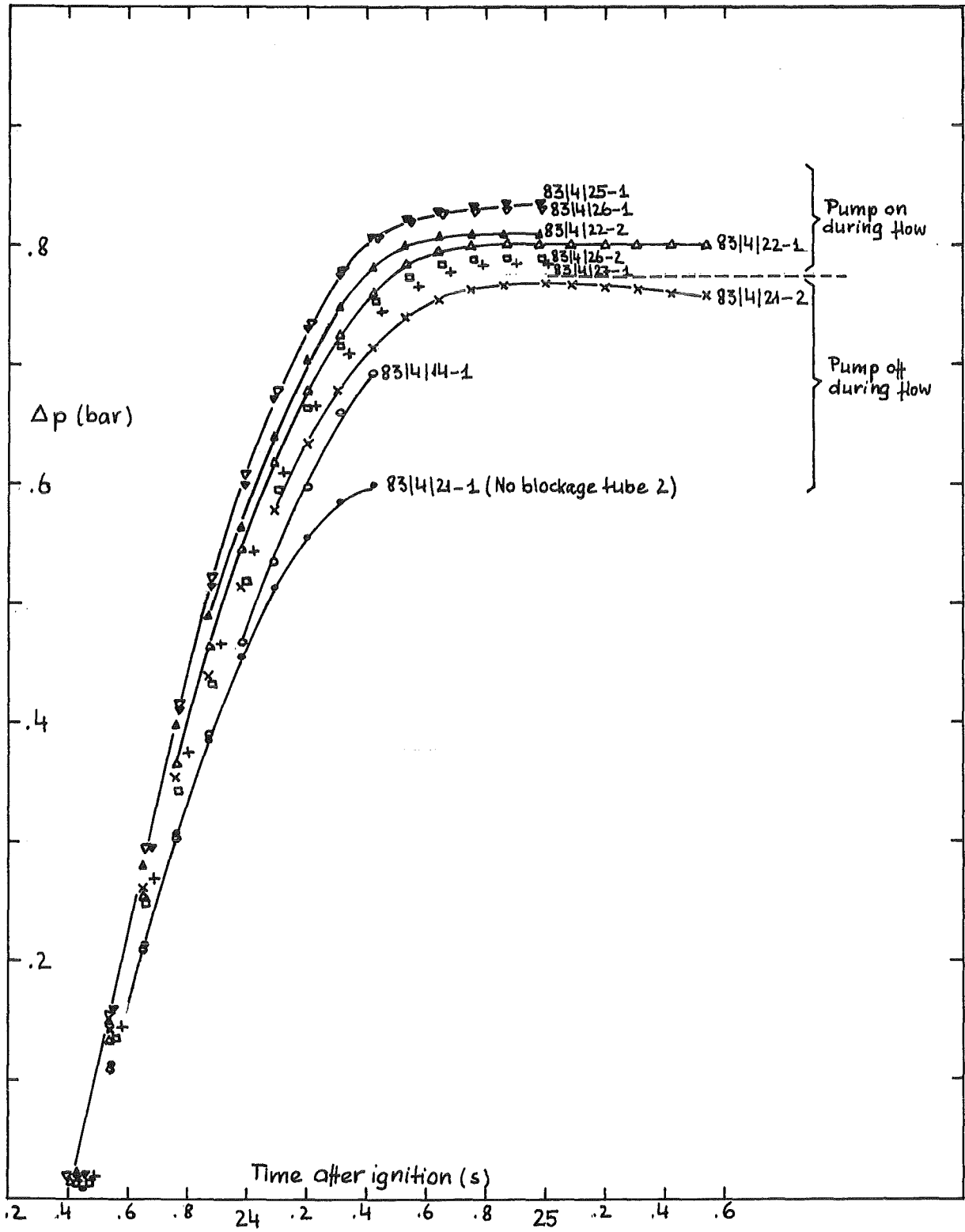


Fig. 17 Series "4 tubes", pressure difference

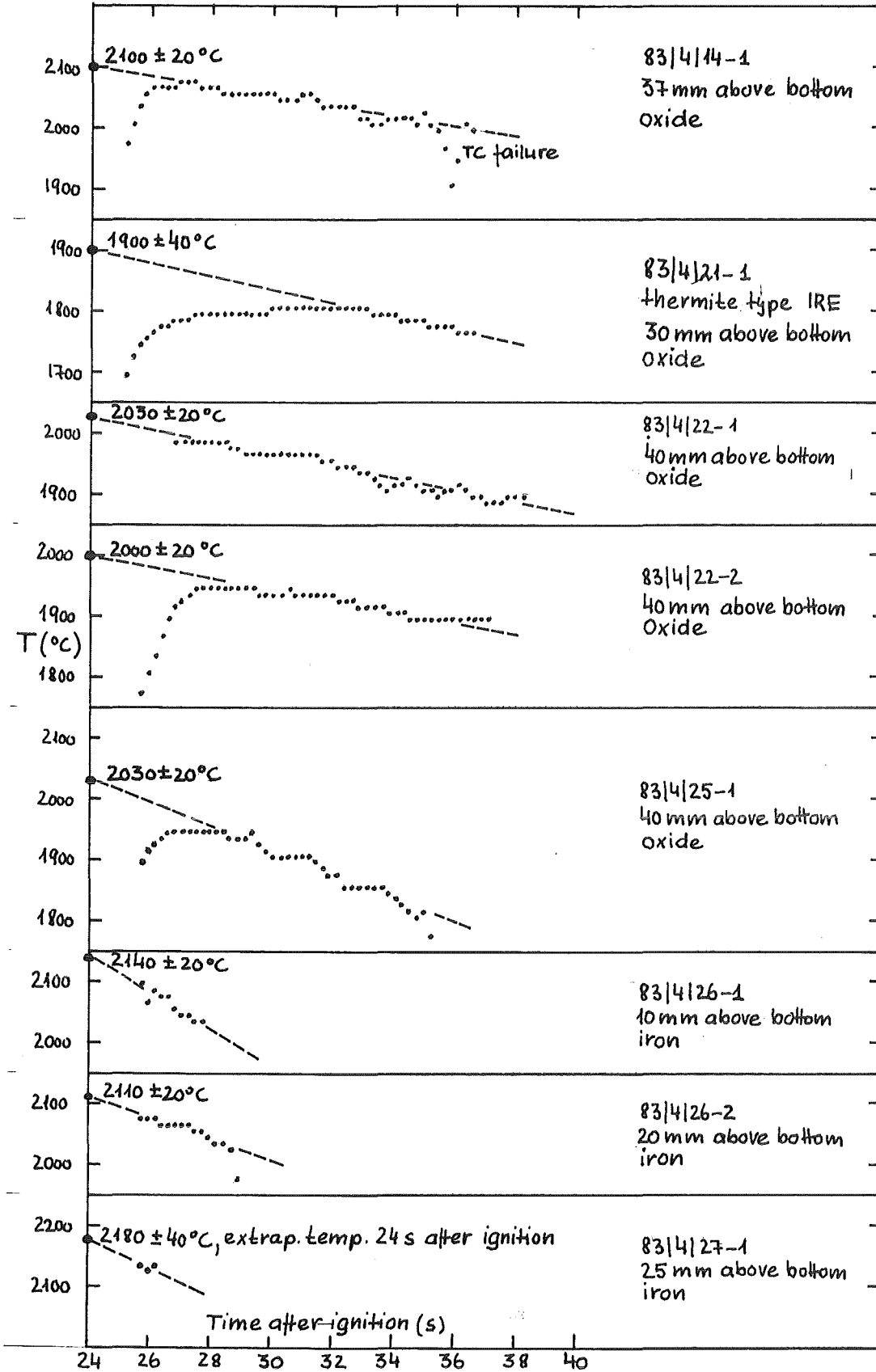


Fig. 18 Series "4 tubes", melt temperature measured with W3Re/W25Re thermocouples

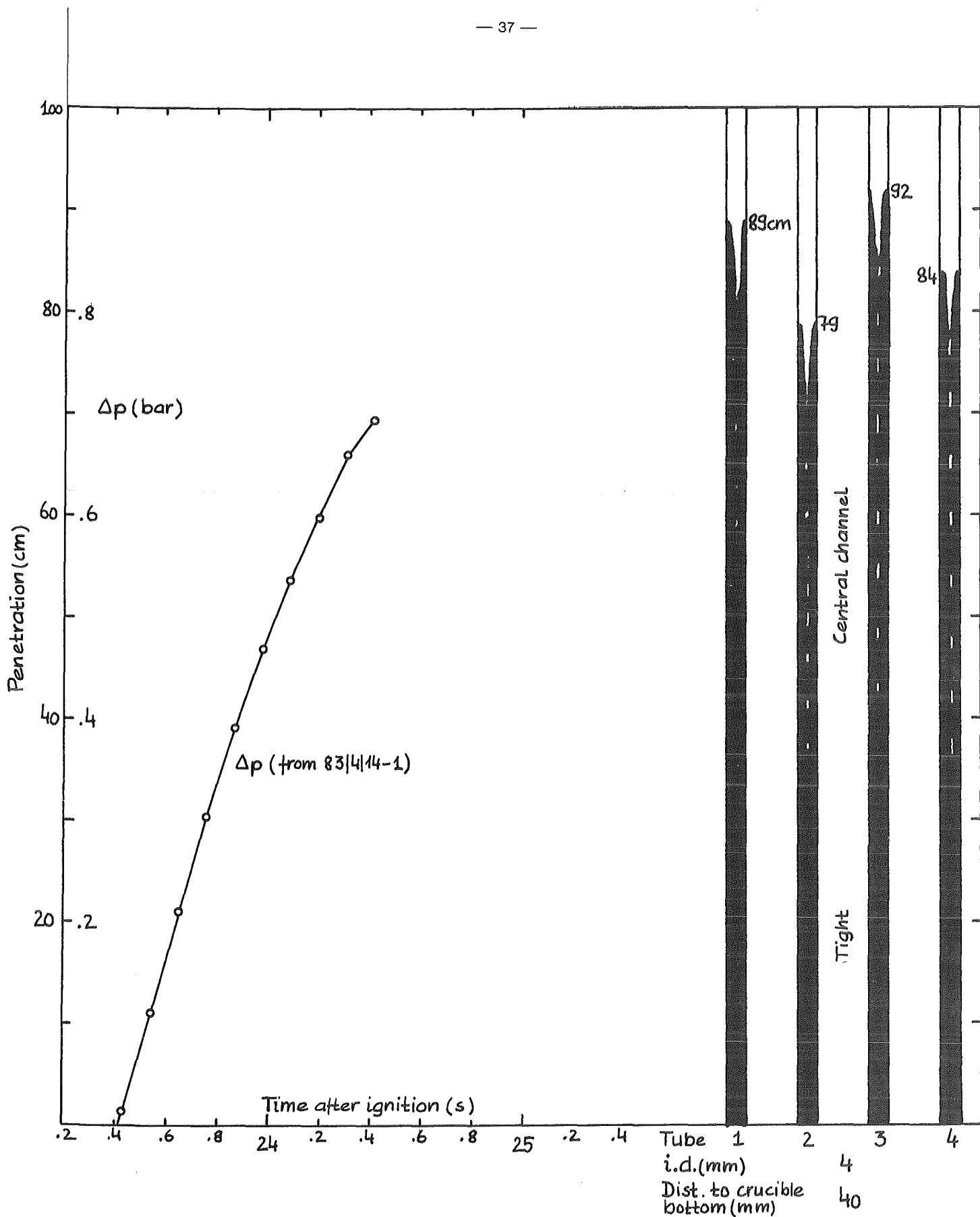


Fig. 19 Series "4 tubes", test 83/3/24-1
 Tubes: Wall 1 mm, length 100 cm; 100 g thermite
 Dip in 23 s after ignition
 Melt: Oxide, estimated $T = 2040 \pm 50$ °C (24 s)
 Pressure difference assumed to be equal as in test
 83/4/14-1

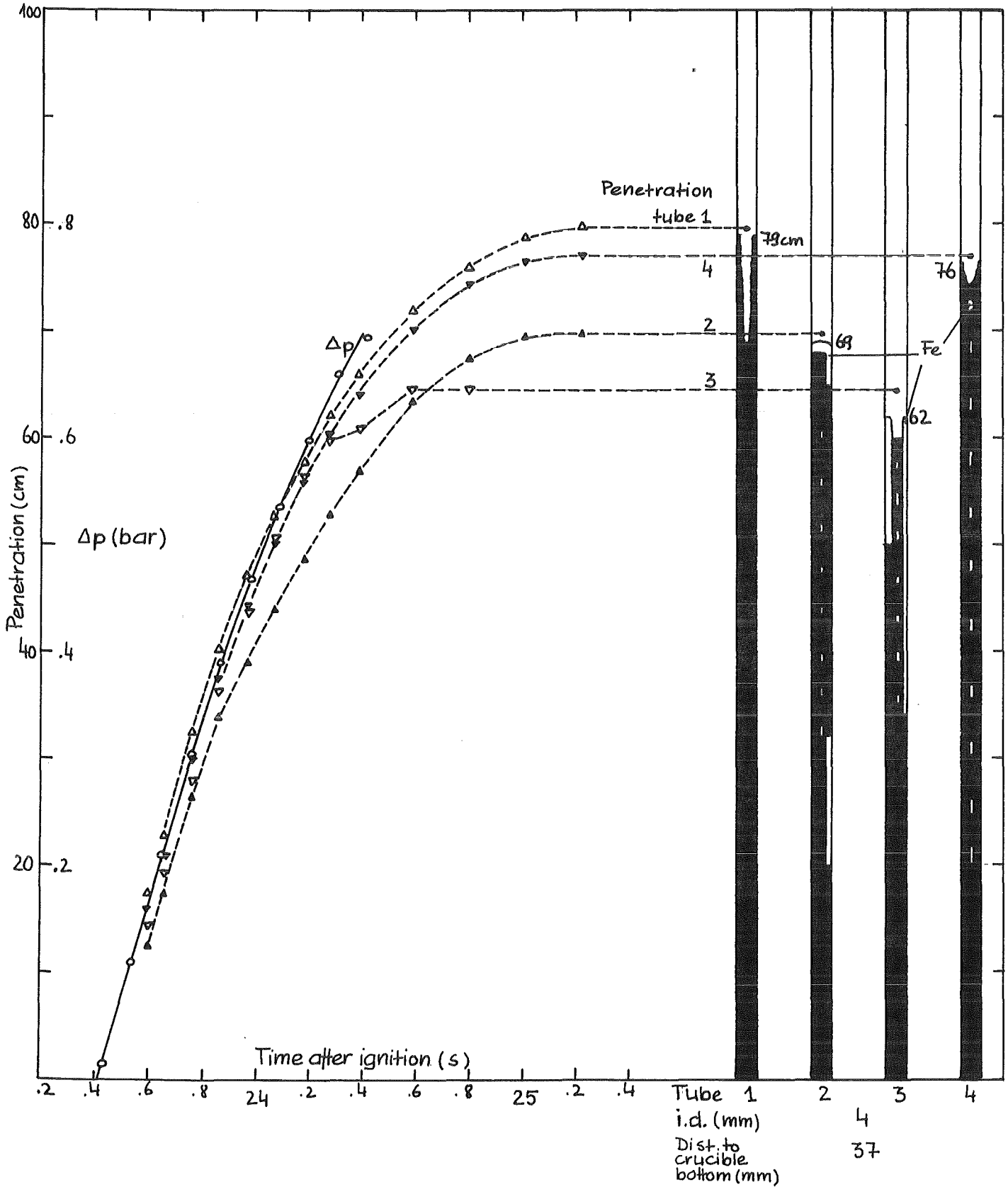


Fig. 20 Series "4 tubes", test 83/4/14-1
 Tubes: Wall 1 mm, length 100 cm; 1000 g thermite
 Dip in 23 s after ignition
 Melt: Oxide (+ some iron), $T = 2100 \pm 20$ °C (24 s,
 37 mm above bottom)

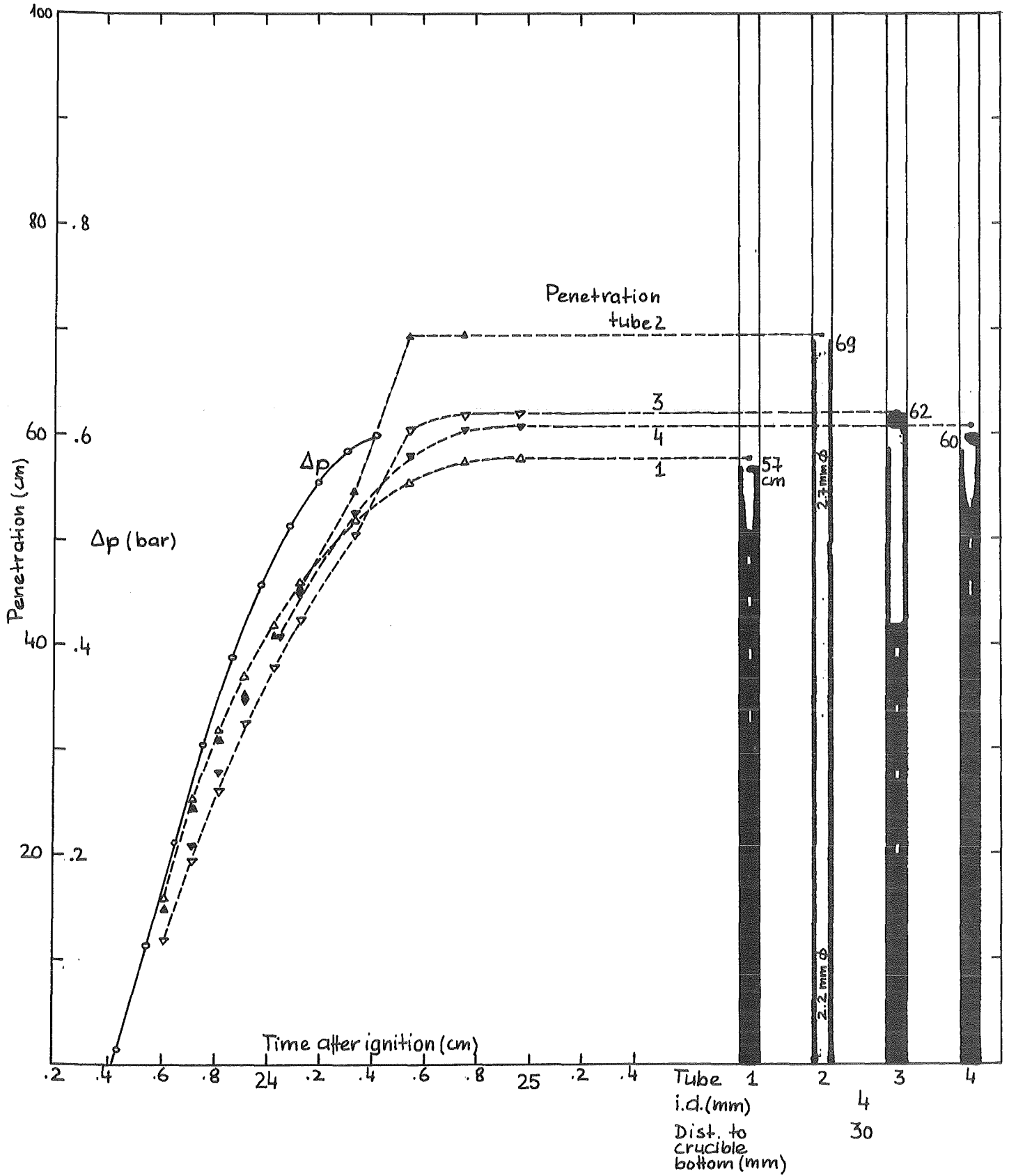


Fig. 21 Series "4 tubes", test 83/4/21-1
 Tubes: Wall 1 mm, length 100 cm
 Dip in 23 s after ignition
 Melt: Oxide, $T = 1900 \pm 40$ °C (24 s, 30 mm above bottom)
 Different thermite (type IRE, 600 g)

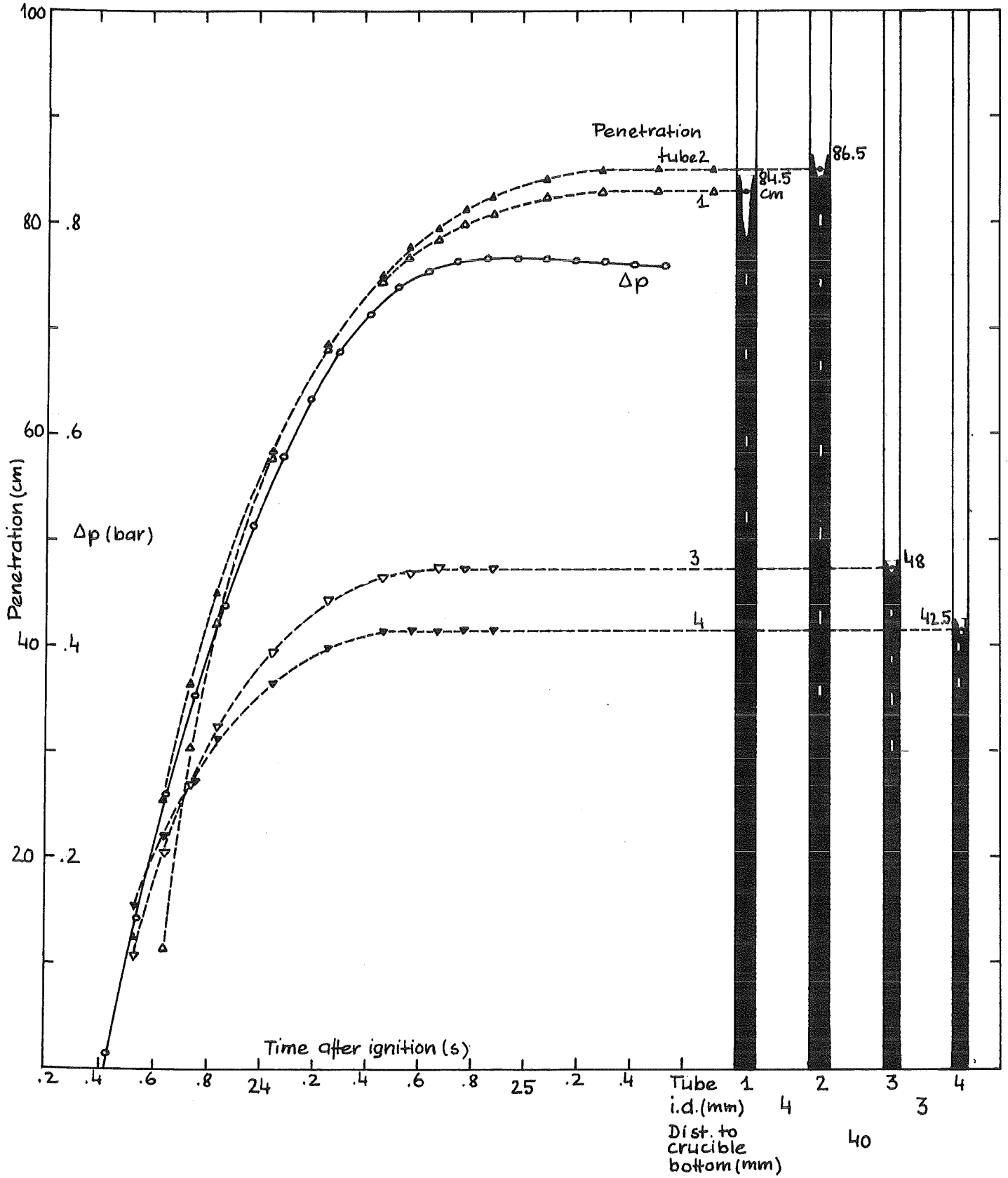


Fig. 22 Series "4 tubes", test 83/4/21-2
 Tubes: Wall 1 mm, length 100 cm; 1000 g thermite
 Dip in 23 s after ignition
 Melt: Oxide, estimated ($= 2040 \pm 50$ °C (24 s))

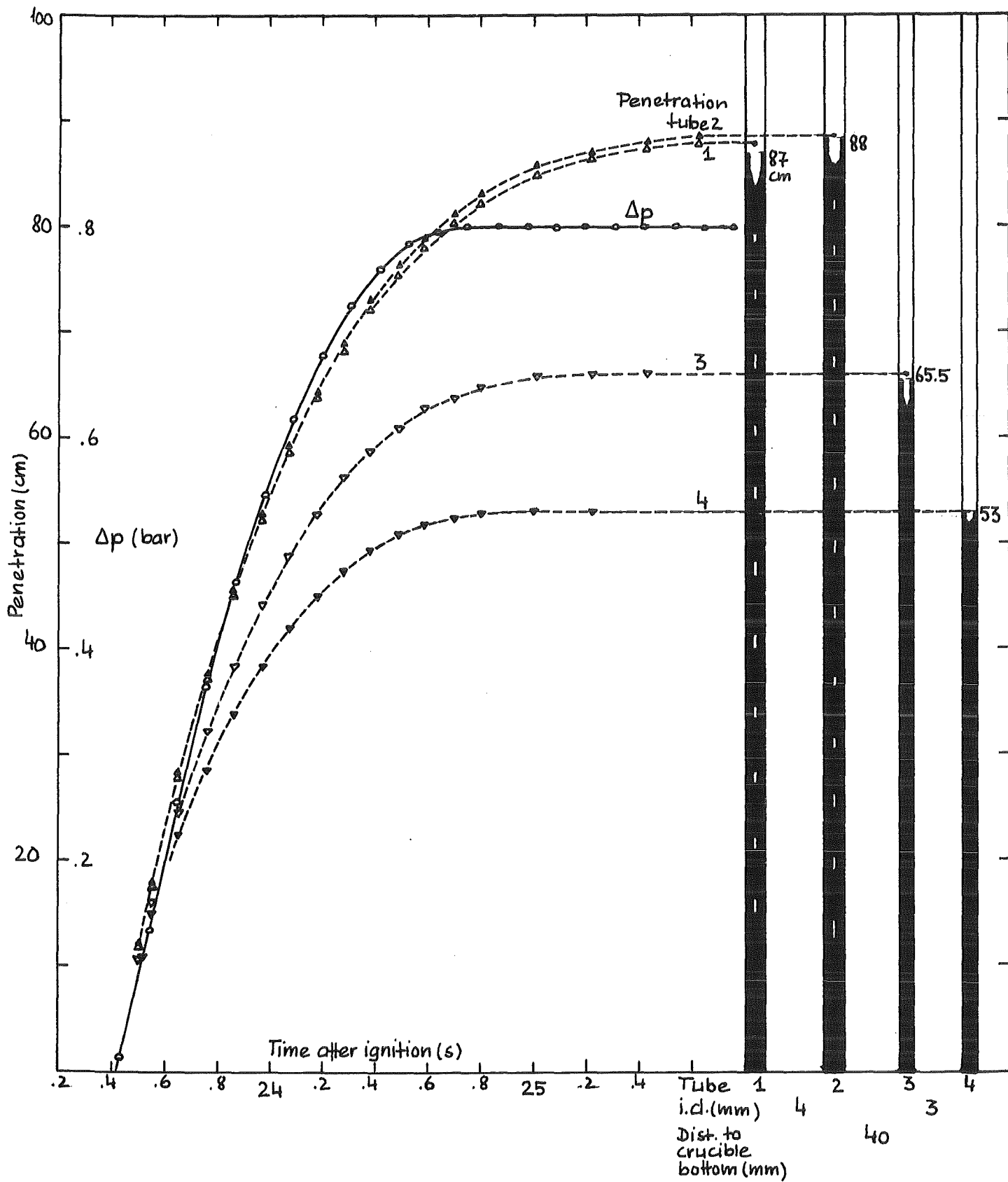


Fig. 23 Series "4 tubes", test 83/4/22-1

Tubes: Wall 1 mm, length 100 cm; 1000 g thermite

Dip in 23 s after ignition

Melt: Oxide, $T = 2030 \pm 20$ °C (24 s, 40 mm above bottom)

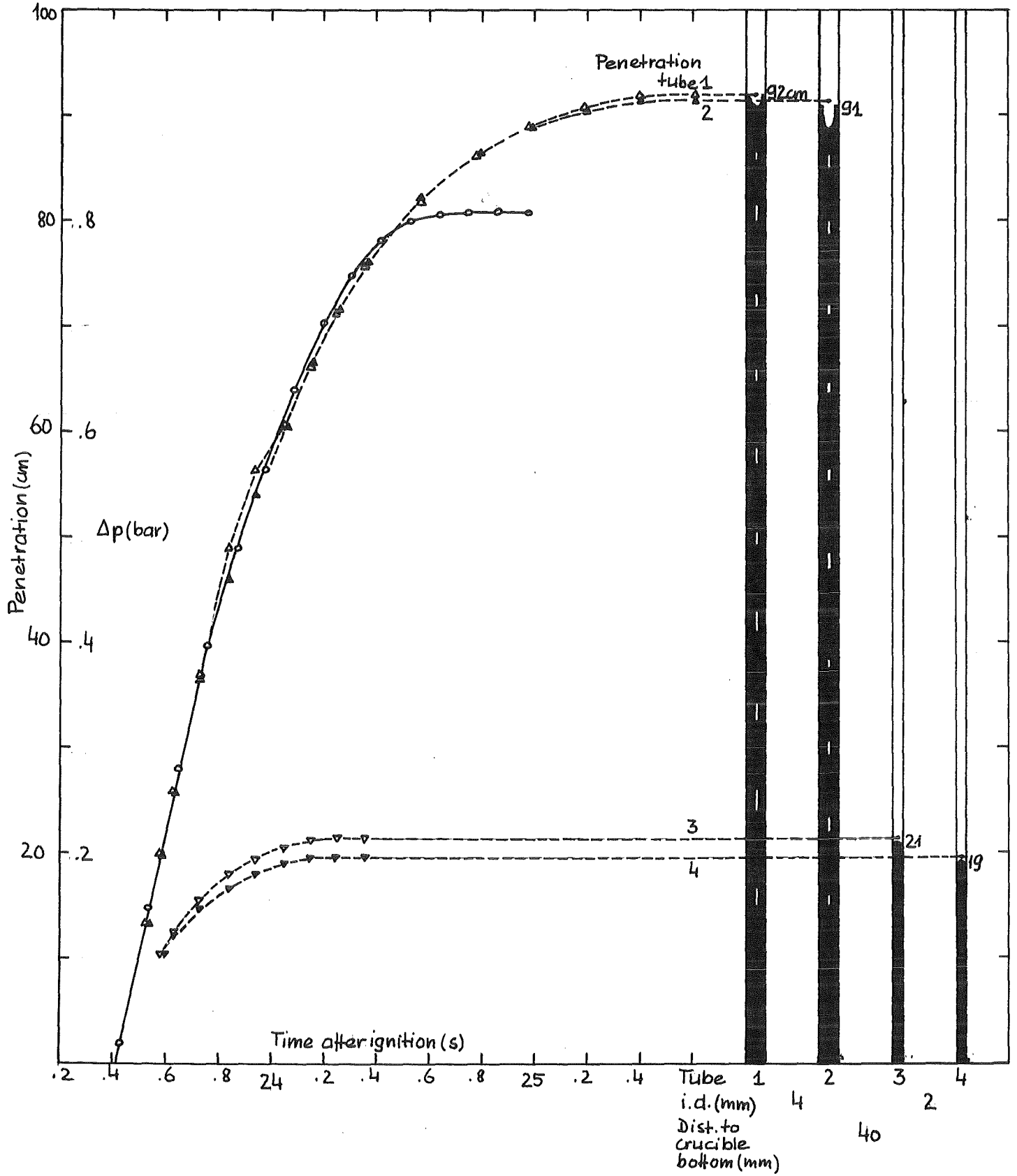


Fig. 24 Series "4 tubes", test 83/4/22-2
 Tubes: Wall 1 mm, length 100 cm; 1000 g thermite
 dip in 23 s after ignition
 Melt: Oxide, $T = 2000 \pm 20$ °C (24 s, 40 mm above bottom)

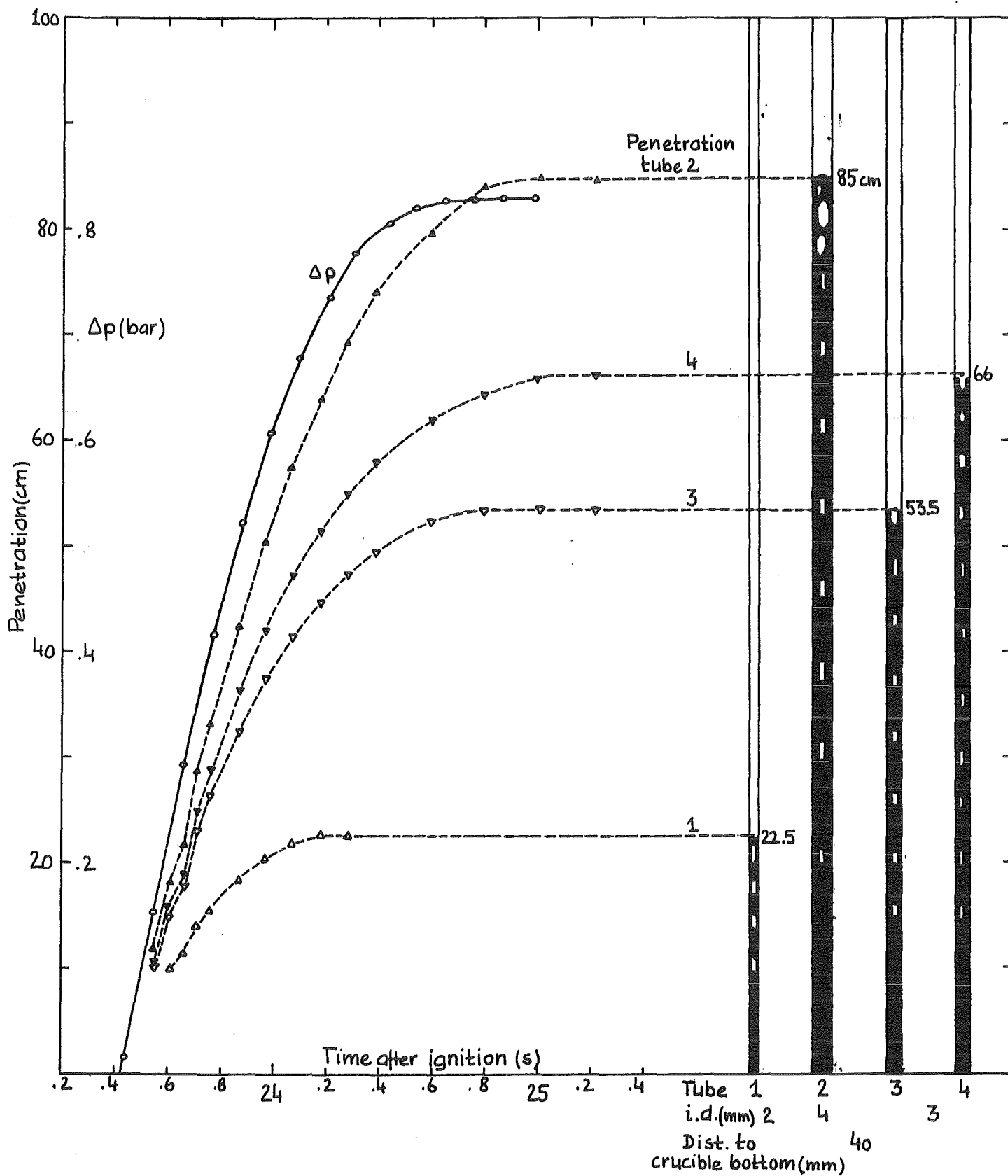


Fig. 25 Series "4 tubes", test 83/4/25-1
 Tubes: Wall 1 mm, length 100 cm; 1000 g thermite
 Dip in 23 s after ignition
 Melt: Oxide, $T = 2030 \pm 20$ °C (24 s, 40 mm above bottom)

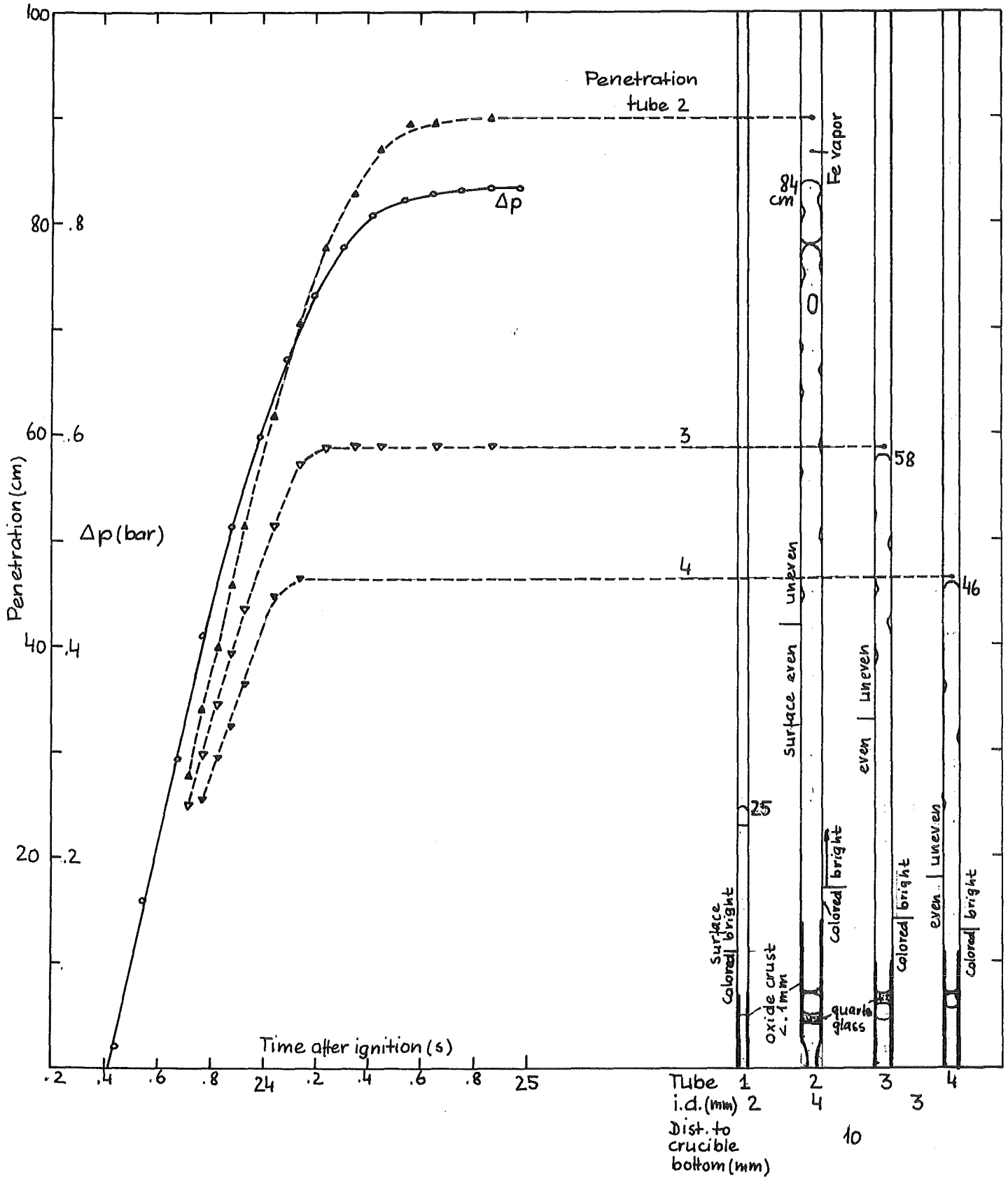


Fig. 26 Series "4 tubes", test 83/4/26-1
 Tubes: Wall 1 mm, length 100 cm; 1000 g thermite
 Dip in 23 s after ignition
 Melt: Iron, $T = 2140 \pm 20$ °C (24 s, 10 mm above bottom)
 Tube inlet deformed

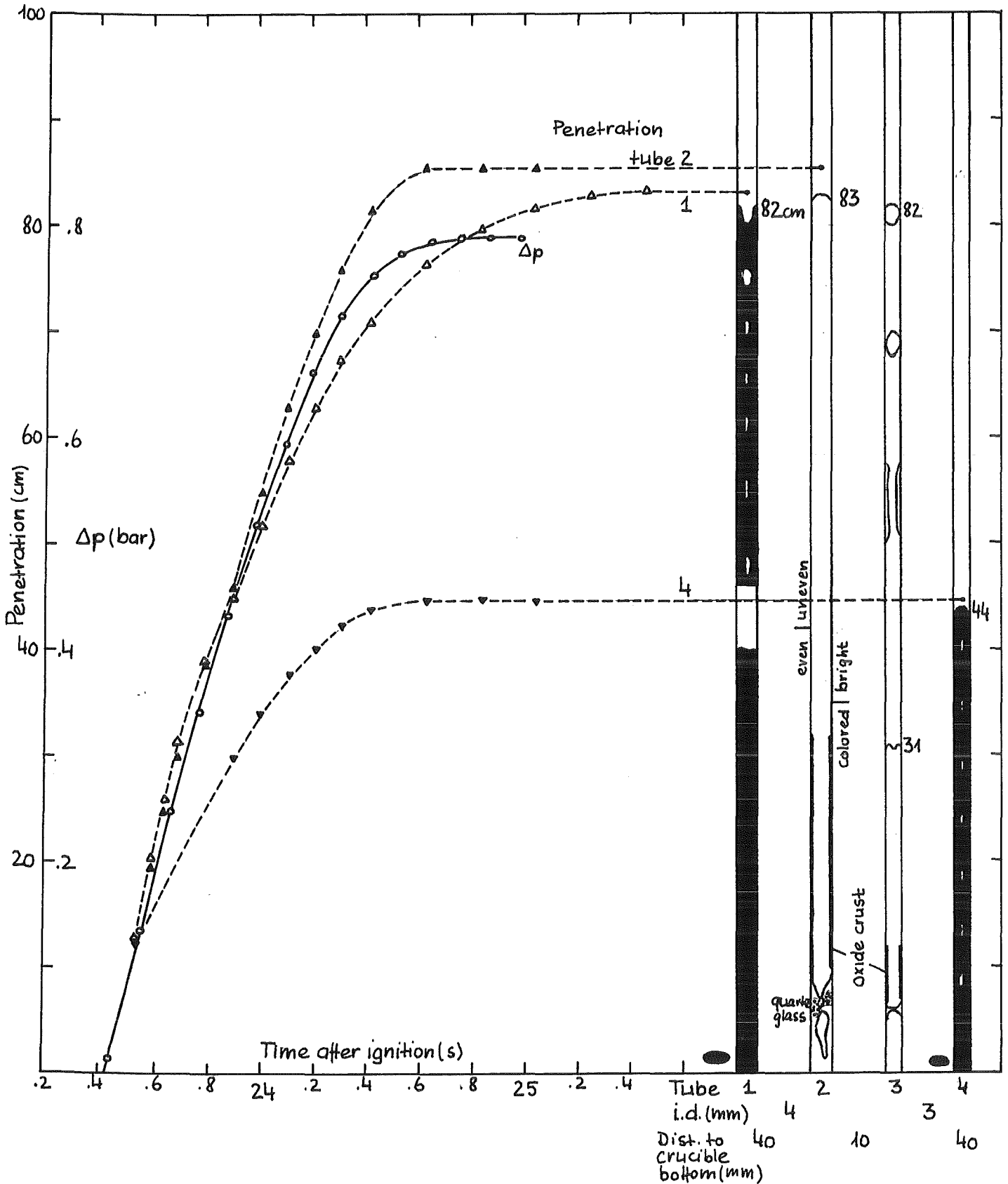


Fig. 27 Series "4 tubes", test 83/4/26-2

Tubes: Wall 1 mm, length 100 cm; 1000 g thermite

Dip in 23 s after ignition

Melt: Oxide

Iron, $T = 2110 \pm 20$ °C (24 s, 20 mm above bottom)

Tube inlet deformed

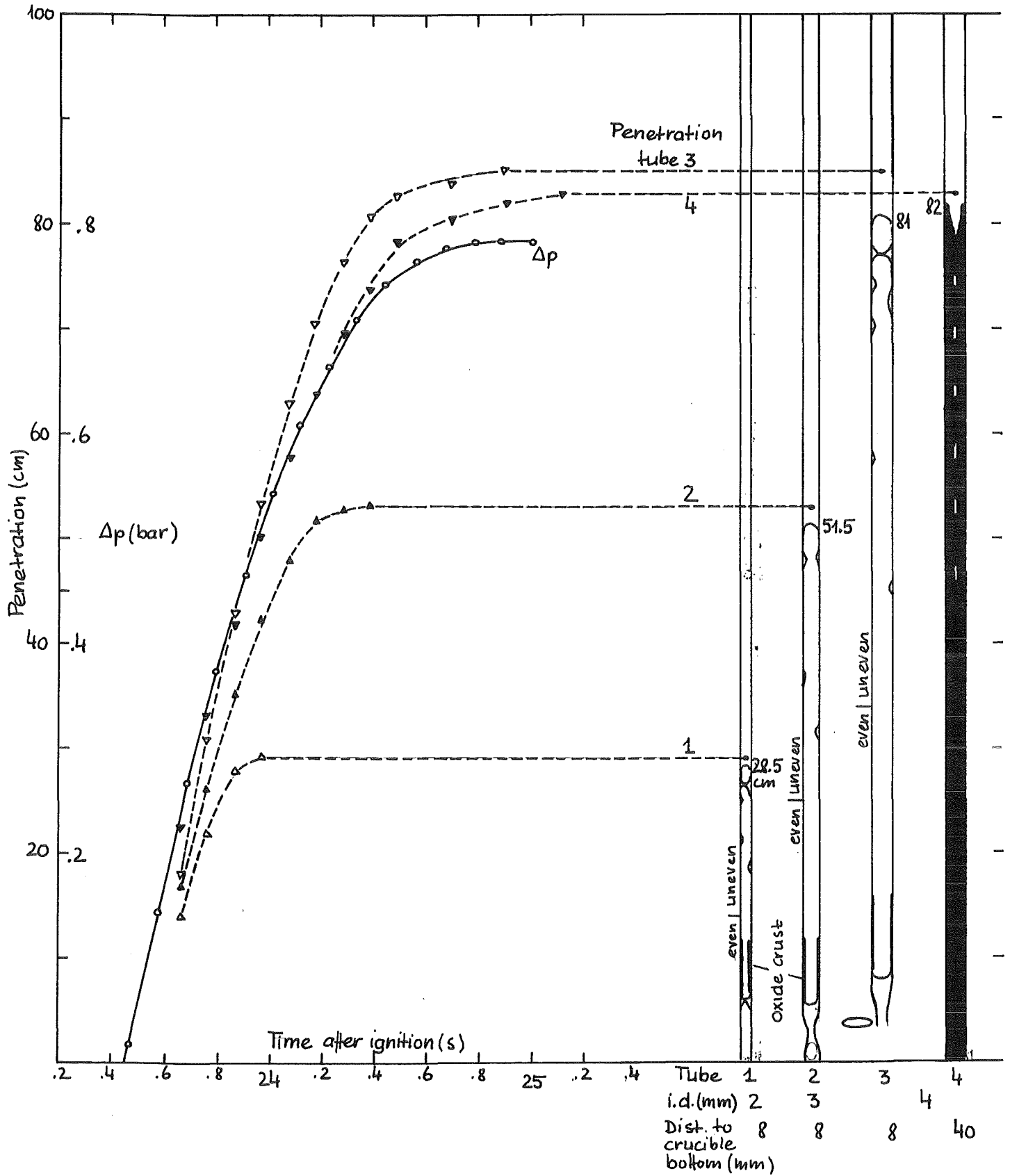


Fig. 28 Series "4 tubes", test 83/4/27-1
 Tubes: Wall 1 mm, length 100 cm; 1000 g thermite
 Dip in 23 s after ignition
 Melt: Oxide
 Iron, $T = 2180 \pm 40$ °C (24 s, 25 mm above bottom)
 Tube inlet deformed

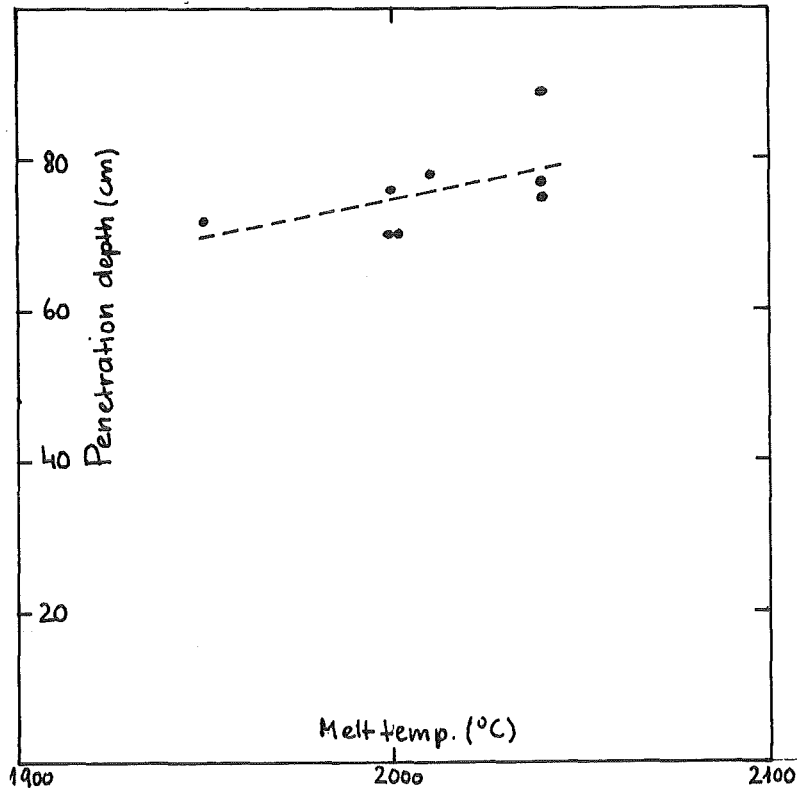


Fig. 29 Penetration depth versus melt temperature
Oxide, channel diameter 4 mm, series "3 tubes"
with $.64 \leq \Delta p/\Delta t \leq .78$ bar/s, thermite type 10/R70-SSH

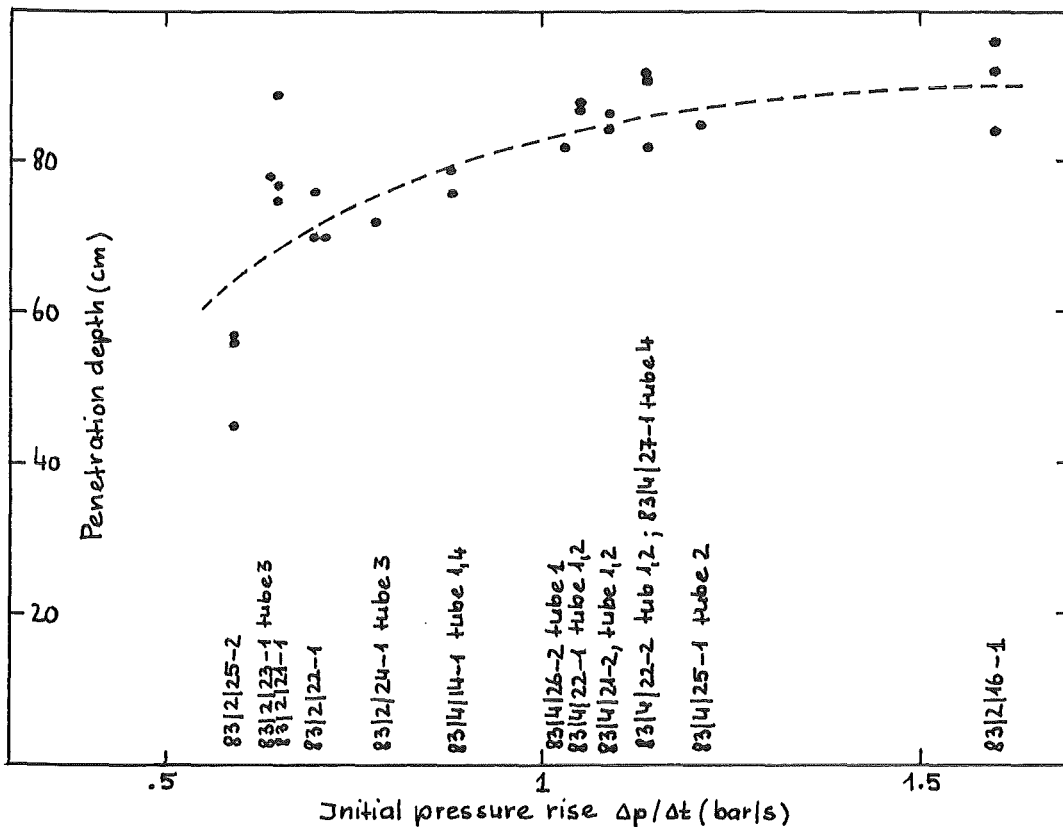


Fig. 30 Penetration depth versus initial pressure rise
Oxide, channel diameter 4 mm, thermite type 10/R70-SSH

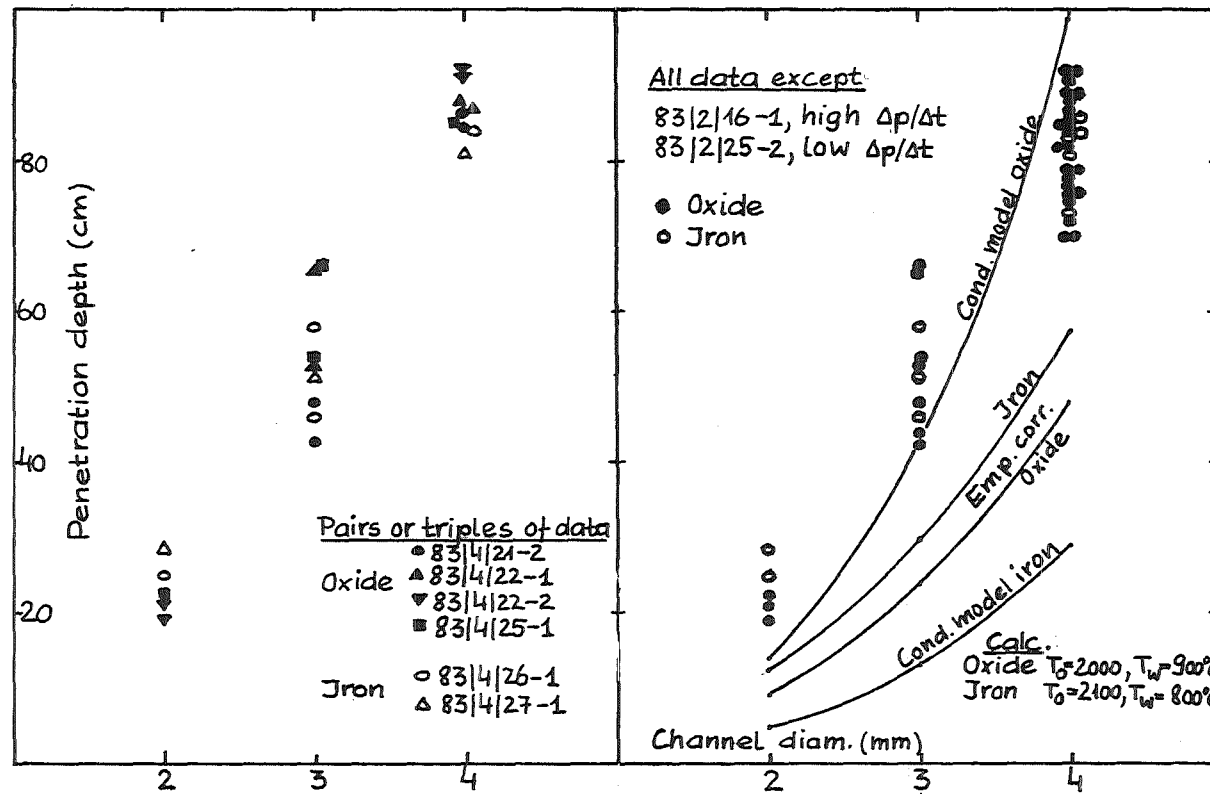


Fig. 31 Penetration depth versus channel diameter
 Thermite type 10/R70-SSH, tests with mixed oxide/iron
 flow omitted